



**HAL**  
open science

# Spontaneous imbibition dynamics in two-dimensional porous media: a generalized interacting multi-capillary model

Shabina Ashraf, Yves Meheust, Jyoti Phirani

► **To cite this version:**

Shabina Ashraf, Yves Meheust, Jyoti Phirani. Spontaneous imbibition dynamics in two-dimensional porous media: a generalized interacting multi-capillary model. *Physics of Fluids*, 2023, 35, pp.012005. 10.1063/5.0123229 . insu-03895688

**HAL Id: insu-03895688**

**<https://insu.hal.science/insu-03895688>**

Submitted on 13 Dec 2022

**HAL** is a multi-disciplinary open access archive for the deposit and dissemination of scientific research documents, whether they are published or not. The documents may come from teaching and research institutions in France or abroad, or from public or private research centers.

L'archive ouverte pluridisciplinaire **HAL**, est destinée au dépôt et à la diffusion de documents scientifiques de niveau recherche, publiés ou non, émanant des établissements d'enseignement et de recherche français ou étrangers, des laboratoires publics ou privés.



Distributed under a Creative Commons Attribution 4.0 International License

# Spontaneous imbibition dynamics in two-dimensional porous media: a generalized interacting multi-capillary model

**Accepted Manuscript:** This article has been accepted for publication and undergone full peer review but has not been through the copyediting, typesetting, pagination, and proofreading process, which may lead to differences between this version and the Version of Record.

Cite as: Physics of Fluids (in press) (2022); <https://doi.org/10.1063/5.0123229>

Submitted: 29 August 2022 • Accepted: 09 December 2022 • Accepted Manuscript Online: 10 December 2022

 Shabina Ashraf,  Yves Meheust and  Jyoti Phirani



View Online



Export Citation



CrossMark

## ARTICLES YOU MAY BE INTERESTED IN

[Numerical study on the pulsating energy evolution in the cavitating flow around a mini Cascade](#)

Physics of Fluids **34**, 123308 (2022); <https://doi.org/10.1063/5.0122844>

[The effect of ribs on the sound radiation directivity of rectangular plates](#)

Physics of Fluids **34**, 122109 (2022); <https://doi.org/10.1063/5.0127918>

[Multiphysics modeling of femtosecond laser-copper interaction: from electron dynamics to plasma eruption](#)

Physics of Fluids (2022); <https://doi.org/10.1063/5.0131001>



## Physics of Fluids

### Special Topic: Food Physics

**Submit Today!**

# Spontaneous imbibition dynamics in two-dimensional porous media: a generalized interacting multi-capillary model

Shabina Ashraf,<sup>1</sup> Yves Méheust,<sup>1</sup> and Jyoti Phirani<sup>2, a)</sup>

<sup>1</sup>*Univ. Rennes, CNRS, GoscienceRennes – UMR6118, F – 35000Rennes, France*

<sup>2</sup>*Department of Civil and Environmental Engineering, University of Strathclyde, Glasgow.*

(Dated: 7 December 2022)

The capillary bundle model, wherein the flow dynamics of a porous medium is predicted from that of a bundle of independent cylindrical tubes/capillaries whose radii are distributed according to the medium's pore size distribution, has been used extensively. But, as it lacks interaction between the flow channels, this model fails at predicting complex flow configuration, including those involving two-phase flow. We propose here to predict spontaneous imbibition in quasi-two-dimensional (quasi-2D) porous media from a model based on a planar bundle of interacting capillaries. The imbibition flow dynamics, and in particular, the breakthrough time, the global wetting fluid saturation at breakthrough, and which capillary carries the leading meniscus, are governed by the distribution of the capillaries' radii and their spatial arrangement. For an interacting capillary system consisting of 20 capillaries, the breakthrough time can be 39% smaller than that predicted by the classic, non-interacting, capillary bundle model of identical capillary radii distribution, depending on the spatial arrangement of the capillaries. We propose a stochastic approach to use this model of interacting capillaries for quantitative predictions. Comparing bundles of interacting capillaries with the same capillary diameter distribution as that of the pore sizes in the target porous medium, and computing the average behavior of a randomly-chosen samples of such interacting capillary bundles with different spatial arrangements, we obtain predictions of the position in time of the bulk saturating front, and of that of the leading visible leading front, that agree well with measurements taken from the literature. This semi-analytical model is very quick to run and could be useful to provide fast predictions on one-dimensional spontaneous imbibition in porous media whose porosity structure can reasonably be considered two-dimensional, e.g., paper, thin porous media in general, or layered aquifers.

## I. INTRODUCTION

When a wetting fluid is placed in contact with a porous medium, the fluid spontaneously imbibe into the pore space due to capillary suction. Such spontaneous imbibition in the porous matrix is crucial for applications such as oil recovery from reservoirs<sup>1-3</sup>, Paper Analytic Devices ( $\mu$ PADS)<sup>4,5</sup>, textiles<sup>6</sup>, inkjet printing<sup>7,8</sup>, microfluidics<sup>9-13</sup>, lab-on-chip devices<sup>14,15</sup>, point-of-care diagnostics<sup>16,17</sup>, Polymer Electrolyte Membrane Fuel Cell (PEMFC)<sup>18,19</sup>, micro heat pipes<sup>20,21</sup>, in understanding the motion of blood cells<sup>22</sup> and in the design of bio-inspired drainage and ventilation systems<sup>23</sup>. Capillary driven imbibition in a homogeneous porous medium follows diffusive dynamics, where the imbibition length is proportional to the square root of time<sup>24-26</sup>. This kind of dynamics was first characterized by Lucas<sup>27</sup> and Washburn<sup>28</sup> for a horizontal cylindrical capillary tube: during the spontaneous imbibition of a wetting fluid of viscosity  $\mu$  in a tube of radius  $r$ , the imbibition length (which here is simply the longitudinal position of the meniscus along the tube) is given by

$$l = \sqrt{\frac{r\sigma \cos \theta_w}{2\mu} t}, \quad (1)$$

where  $\sigma$  is the surface tension coefficient and  $\theta_w$  is the wetting angle of the invading fluid on the tube's wall. In Eq. (1), the prefactor of the  $\sqrt{t}$  law is proportional to  $\sqrt{r}$ , which implies that at any given time the meniscus will have advanced

more along a capillary of larger radius than along one of smaller radius. Later, the phenomenon of imbibition in a single pore/tube was observed to be strongly dependent on the geometries of the capillaries<sup>29-40</sup>.

Due to the similarity in the macroscopic laws describing the time evolution of the imbibition length between imbibition in a capillary tube and imbibition in a homogeneous porous medium, the capillary bundle model, considering a bundle of non-interacting capillaries of different radii, is classically considered as a proxy for porous media, in particular, soils<sup>41-44</sup>. However, in a naturally occurring porous medium, the pores are of various shapes and sizes, and are interconnected<sup>45,46</sup>. In a quasi-two-dimensional (2D) porous medium such as paper, Bico and Quéré<sup>47</sup> showed that there are two imbibing fronts, a leading front in the small pores and a bulk saturating front which lags behind, which is contradictory to the predictions of the classic bundle of (non-interacting) capillaries, where the pores with larger radii have the leading front during imbibition.

The model geometry consisting of interacting capillaries (i.e., a capillary bundle where an opening allowing fluid exchange exists between adjacent capillaries, see e.g. Ref.55) accounts for the effect of the interaction between pores on the pore scale flow dynamics, which in turn affects the Darcy scale flows in porous media<sup>48-55</sup>. In a system of two interacting capillaries, the imbibition in the capillary of smaller radius is found to be faster than that in the one of larger radius, unlike the behavior suggested by Eq. (1). However, a majority of these models were limited to predicting the imbibition dynamics in an ordered arrangement of pores or in two and three interacting capillary systems. For a system consisting of three interacting non-cylindrical capillaries, Unsal

<sup>a)</sup>Electronic mail: jyoti.phirani@strath.ac.uk

et al.<sup>56–58</sup> showed experimentally that the imbibition speed is fastest in the capillary of least effective radius. On the contrary, Ashraf et al.<sup>55</sup>, using a one-dimensional lubrication approximation model and considering a system of three interacting cylindrical capillaries, showed that imbibition is not always fastest in the capillary of smallest radius. Furthermore, both these studies<sup>55,56</sup> showed that, for three capillary systems, the random positioning of the capillaries strongly impacts the invasion behaviour. But how the interconnection between capillaries impacts the overall imbibition dynamics is far from being fully understood in the general case of a larger number of tubes. Consequently, interacting capillary systems, despite having a complexity which is intermediate between that of the classical bundle of non-interacting capillaries, have so far not been used to predict the generalized imbibition phenomenon observed in porous media consisting of several pores of irregular sizes and varying connectivity. To this aim, more complex models have been introduced since based on pore-network geometries inferred from a geometrical analysis of the porous medium in which imbibition is to be investigated<sup>59–61</sup>. We will present here a model of intermediate complexity between those early interacting-capillary models and pore network models. Note that in many practical cases, the detailed porous structure is not known, and only an estimate of the pore size distribution is available; in such cases a pore network model cannot be applied without making assumptions on the unknown structure, whereas the model presented here can be applied directly.

We thus propose a generalized one-dimensional model to predict spontaneous imbibition in a capillary bundle consisting of any number of randomly arranged cylindrical tubes that interact with each other, with any arbitrary distribution of the capillaries' radii. The model generalizes the study by Ashraf et al.<sup>55</sup> for systems of two and three interacting capillaries to an arbitrary number of interacting capillaries. It is meant to model spontaneous imbibition in quasi-2D porous media for which the pore size distribution is known. The model is inspired from a model developed to tackle spontaneous imbibition in stratified geological porous media<sup>62</sup>. The two models are formally very similar to each other, but, due to the difference in geometries (flat layers for the stratified geological formation, cylindrical tubes in the present model), the equations are not identical. More importantly, the two studies differ widely in that the relative positioning of the layers in a geological medium is given, whereas, for a quasi-2D porous medium whose pore size distribution is known, the relative positioning of connected capillaries of different diameters within the 2D bundle that can predict the medium's behavior is not known a priori. Here, we explain the underlying physical phenomena causing the menisci to advance at different rates in the different capillaries, and demonstrate that both the spatial arrangement of the interacting capillaries, and for a given arrangement, the contrasts in the capillaries' radii (i.e., their ratios), are crucial in predicting the imbibition dynamics. In contrast to the standard (non-interacting) capillary bundle, this model provides predictions that are qualitatively consistent with the phenomenology of spontaneous imbibition in real (quasi)-two-dimensional (2D) porous media. In

particular, this model correctly predicts that the smaller pores carry the leading front, while the larger pores carry the lagging saturating front responsible for the mass uptake of fluid in the porous medium, as measured in a paper-based porous medium<sup>47</sup>. Furthermore, we provide a successful quantitative comparison between the measurements of Bico & Quéré on the leading and lagging imbibition fronts to predictions of the model obtained using a stochastic approach: the predicted behavior is the average of those obtained for all possible spatial organizations of the capillaries' diameter distribution. Though less accurate than fully numerical (and much more complicated) pore network models, this semi-analytical model has the advantage of running within seconds on any computer.

The presentation is organized as follows. We first review the model by Ashraf et al.<sup>55</sup> (section II A). We then proceed to extend it to a system consisting of 4 interacting capillaries (section II B), before presenting the generalized one-dimensional model predicting spontaneous imbibition in an interacting multi-capillary system (section II C). We then examine the imbibition dynamics in a system of four interacting capillaries (section III A) and in a similar system consisting of 20 capillaries (section III B). In the discussion, we first compare the predictions of our model to those of the classic, non-interacting, capillary bundle (section III C 1), and, finally, confront its predictions of the leading and lagging fronts in a real quasi-2D porous medium from the literature to the published experimental measurements (section III C 2). Section IV contains a summary of the work and conclusive remarks, and discusses prospects to this study.

## II. MODELS

### A. Capillary imbibition in interacting capillaries

Using the capillary system shown in Fig. 1, Ashraf et al.<sup>55</sup> used volume of fluid<sup>63</sup> (VOF) two-phase flow simulations to study spontaneous imbibition in a bundle of two or three interacting capillaries. These CFD (computational fluid dynamics) calculations provided the entire pressure and velocity fields inside the connected capillaries. They showed that (1) the invading wetting fluid transfers between two adjacent capillaries from the capillary of larger radius to that of smaller radius, but this transfer occurs only in the immediate vicinity of the (less advanced) meniscus of the capillary of larger radius; (2) that everywhere else (that is, everywhere except in the vicinity of that meniscus), the flow in the capillaries is not perturbed by the transfer of fluid between the capillaries; and (3) that, consequently, the pressure can be considered uniform over all transverse sections of the capillary system where both capillaries are filled with the same fluid, since no flow occurs along the transverse direction (if one neglects the small regions in the vicinity of the less advanced meniscus). These findings (1-3) served as basic assumptions to develop a reduced order, Washburn-like one dimensional model for a bundle of two and three interacting capillaries that can interact hydrodynamically with the neighbouring capillaries along their touching sides. The model predicted that in a bundle of two interact-

192 ing capillaries the meniscus in the capillary of smaller radius  
 193 moves ahead of the other one during the spontaneous imbibi-  
 194 tion, in consistency with the results of the VOF simulations.  
 195 In this study we shall generalize the reduced order model of  
 196 Ashraf et al.,<sup>55</sup> to an arbitrary number of capillaries positioned  
 197 in the same plane and interacting with their neighbours.

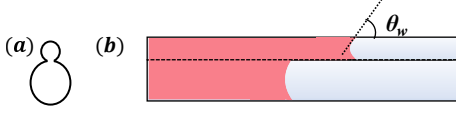


FIG. 1. Spontaneous imbibition in two interacting capillaries, (a) cross-sectional view, (b) lateral view showing the contact angle  $\theta_w$ .

198  
 199 For a flat bundle of three interacting capillaries, the model  
 200 of Ashraf et al.,<sup>55</sup> showed that the distribution of radii and the  
 201 spatial arrangement of the capillaries impact the imbibition  
 202 behavior in the capillary system significantly. The meniscus  
 203 in the capillary of smallest radius does not always move ahead  
 204 of the others. 244

205  
 206 In the following sections, we examine the dynamics of  
 207 menisci during spontaneous imbibition in a flat bundle con-  
 208 taining an arbitrary number of interacting capillaries. This  
 209 generalization of the interacting capillaries' model follows the  
 210 model development formulations from the study of Ashraf et  
 211 al.,<sup>62</sup> for imbibition in stratified porous media. In a stratified  
 212 porous medium, the contrasts in layer transmissivities and the  
 213 relative positioning of the layers control the imbibition dy-  
 214 namics, whereas in the present interacting capillaries bundle  
 215 model, the positioning of the capillaries also plays a crucial  
 216 role, but the role played by the transmissivities in the strati-  
 217 fied medium is played by the product of the capillaries' per-  
 218 meabilities by their cross-sectional areas, both of which are  
 219 controlled by the contrasts in the capillaries' radii. 258

220 We first describe below the one-dimensional model formu-  
 221 lation for a system of four interacting capillaries to understand  
 222 the underlying equations, before generalizing the model to  
 223 multiple-interacting capillary system. 262

## 224 B. Model development for four interacting capillaries

225 To predict the dynamics of spontaneous imbibition in a  
 226 porous medium using a system of interacting capillaries, we  
 227 need to take the arrangement of capillaries into account, un-  
 228 like for the classic capillary bundle (sometimes called bundle  
 229 of-tubes) model. For a porous medium made of  $n$  interact-  
 230 ing capillaries, there are  $n!/2$  different arrangements. Fig.  
 231 2 shows a bundle of four interacting capillaries that are or-  
 232 dered spatially according to their radii  $r_\alpha > r_\beta > r_\gamma > r_\delta$ ; we  
 233 call this arrangement  $\alpha\beta\gamma\delta$ . The capillary pressure in tube  
 234 ( $i = \alpha, \beta, \gamma, \delta$ ) is given by the Young-Laplace equation as<sup>64,65</sup>  
 235

$$236 P_{C_i} = \frac{2\sigma \cos \theta_w}{r_i}, \quad (2) \quad 278$$

237 where  $\sigma$  is the surface tension and  $\theta_w$  the contact angle,  
 238 hence,  $P_{C_\alpha} < P_{C_\beta} < P_{C_\gamma} < P_{C_\delta}$ . The corresponding imbibi-  
 239 tion lengths in the tubes at any time  $t$  are denoted respectively

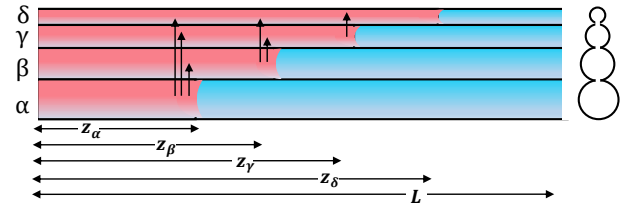


FIG. 2. Schematic showing the spontaneous imbibition in an ordered system of four interacting capillaries. The imbibition lengths in capillaries  $\alpha, \beta, \gamma, \delta$  of radii  $r_\alpha, r_\beta, r_\gamma, r_\delta$  are denoted by  $z_\alpha, z_\beta, z_\gamma, z_\delta$ , respectively. The cross section of the system of interacting capillaries is also shown.

by  $z_i(t)$ . We consider the assumptions from Ashraf et al.<sup>55</sup>, according to which (1) the pressure equilibrates over the sections of the capillary system that are entirely filled with the invading fluid, and (2) fluid transfers from a capillary having a larger radius to an adjacent capillary having a smaller radius just before the meniscus, which in the model we assume to occur at the position of the meniscus. We show this fluid transfer between adjacent capillaries in the vicinity of the meniscus by vertical arrows in Fig. 2. We consider the interaction between the capillaries to be sufficiently low for the Poiseuille flow in each of the capillaries to be maintained. At any given time  $t$ , the less advanced meniscus (i.e., that for which the imbibition length is the smallest) will be in the capillary for which the driving capillary pressure jump across the meniscus is the smallest, hence it will be the meniscus in the  $\alpha$  capillary. For  $z < z_\alpha(t)$ , the pressure field must be identical in all capillaries. Similarly, the next-less-advanced meniscus is necessarily the  $\beta$  capillary driven by the capillary pressure  $P_{C_\beta}$ , so at any time  $t$  the pressure field is identical in capillaries  $\beta, \gamma$  and  $\delta$  for  $z_\alpha(t) < z < z_\beta(t)$ , and so forth: the pressure field is identical in the  $\delta$  and  $\gamma$  capillaries for  $z_\beta(t) < z < z_\gamma(t)$ . The imbibition length in capillary  $\delta$ ,  $z_\delta(t)$  is the largest at any time  $t$ .

We now consider one of the random arrangements as shown in the schematic of Fig. 3, where the order of arrangement of the capillaries is  $\beta\gamma\alpha\delta$ . It was explained by Ashraf et al.,<sup>54</sup> that, for a randomly-arranged interacting capillary system, the meniscus in the smallest radius capillary does not always lead. For this arrangement, depending upon the contrasts in the radii, three different positionings of the menisci are possible as shown in Fig. 3 (a), (b) and (c). At any given time  $t$ , for  $0 < z_\alpha(t)$ , the pressure field is identical in all capillaries, and the pressure drop from the inlet to  $z_\alpha(t)$  is  $P_{C_\alpha}$ . For  $z > z_\alpha(t)$ , the imbimbing fluid is continuous in the capillaries  $\beta$  and  $\gamma$ , since they are connected. Therefore, the pressure field is the same in the capillaries  $\beta$  and  $\gamma$  for  $z_\alpha(t) < z < z_\beta(t)$ . As  $r_\beta > r_\gamma$  (meaning that the capillary suction in  $\beta$  is less than that in  $\gamma$ ), during the spontaneous imbibition,  $z_\beta(t) < z_\gamma(t)$ , at all times. Although the capillary  $\delta$  is filled with the imbimbing phase, the non-wetting fluid in  $\alpha$  disconnects it from capillaries  $\beta, \gamma$  for  $z > z_\alpha(t)$ . Therefore, for  $z > z_\alpha(t)$  the pressure field in  $\delta$  can be different from that in  $\beta, \gamma$ . For the arrangement  $\beta\gamma\alpha\delta$  shown in the schematic of Fig. 3,  $z_\alpha < z_\beta < z_\gamma$  and  $z_\alpha < z_\delta$  during the imbibition process and the position of

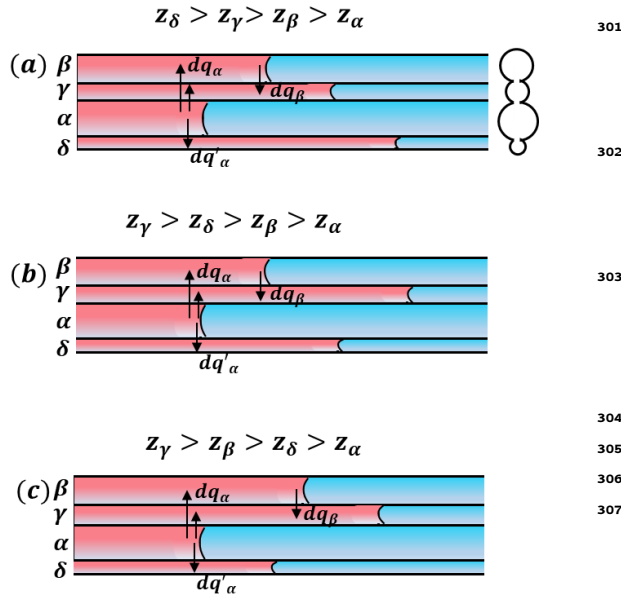


FIG. 3. Spontaneous imbibition in a system of four interacting capillaries with a spatial arrangement of  $\beta\gamma\alpha\delta$  of the capillaries. The imbibition lengths in capillaries  $\alpha$ ,  $\beta$ ,  $\gamma$ ,  $\delta$  of radii  $r_\alpha$ ,  $r_\beta$ ,  $r_\gamma$ ,  $r_\delta$  are  $z_\alpha(t)$ ,  $z_\beta(t)$ ,  $z_\gamma(t)$ ,  $z_\delta(t)$ , respectively. The schematics of the imbibition phenomenon show the fluid transfer at menisci locations with arrows. For this spatial arrangement, depending upon the contrasts in the capillaries' radii, the possible orders in the invasion lengths can be (a)  $z_\alpha < z_\beta < z_\gamma < z_\delta$ , (b)  $z_\alpha < z_\beta < z_\delta < z_\gamma$  and (c)  $z_\alpha < z_\delta < z_\beta < z_\gamma$ . The cross section of the system of interacting capillaries is also shown for (a).

$$Pc_\delta - Pc_\alpha = \frac{8\mu(z_\delta(t) - z_\alpha(t))}{r_\delta^2} \left( \frac{dz_\delta}{dt} \right), \quad (5)$$

$$Pc_\beta - Pc_\alpha = \frac{8\mu(z_\beta(t) - z_\alpha(t))}{r_\beta^4 + r_\gamma^4} \left( r_\beta^2 \frac{dz_\beta}{dt} + r_\gamma^2 \frac{dz_\gamma}{dt} \right), \quad (6)$$

$$Pc_\gamma - Pc_\beta = \frac{8\mu(z_\gamma(t) - z_\beta(t))}{r_\gamma^2} \left( \frac{dz_\gamma}{dt} \right). \quad (7)$$

Eqs. (4) to (7) are rendered non-dimensional by normalizing the positions by the total capillary system's length,  $L$ , and time by  $[8\mu L^2 / (Pc_\alpha r_\alpha^2)]$ , thus defining the non-dimensional positions and times

$$Z_i = \frac{z_i}{L}, \quad i = \alpha, \beta, \gamma, \delta \quad \text{and} \quad T = \frac{Pc_\alpha r_\alpha^2 t}{8\mu L^2}. \quad (8)$$

Introducing the contrasts in radii,  $\lambda_i = r_i/r_\alpha$ , and in capillary pressures,  $\varepsilon_i = Pc_i/Pc_\alpha$ , for  $i = \beta, \gamma, \delta$ , we then obtain the non-dimensional form of Eqs. (4) to (7) as

$$1 = \frac{Z_\alpha}{1 + \lambda_\beta^4 + \lambda_\gamma^4 + \lambda_\delta^4} \left( \frac{dZ_\alpha}{dT} + \lambda_\beta^2 \frac{dZ_\beta}{dT} + \lambda_\gamma^2 \frac{dZ_\gamma}{dT} + \lambda_\delta^2 \frac{dZ_\delta}{dT} \right), \quad (9)$$

$$\varepsilon_\delta - 1 = \frac{Z_\delta - Z_\alpha}{\lambda_\delta^2} \left( \frac{dZ_\delta}{dT} \right), \quad (10)$$

$$\varepsilon_\beta - 1 = \frac{Z_\beta - Z_\alpha}{\lambda_\beta^4 + \lambda_\gamma^4} \left( \lambda_\beta^2 \frac{dZ_\beta}{dT} + \lambda_\gamma^2 \frac{dZ_\gamma}{dT} \right). \quad (11)$$

$$\varepsilon_\gamma - \varepsilon_\beta = \frac{Z_\gamma - Z_\beta}{\lambda_\gamma^2} \left( \frac{dZ_\gamma}{dT} \right), \quad (12)$$

Further assuming that the contact angle  $\theta_w$  is the same in all capillaries, we have  $\varepsilon_i = 1/\lambda_i$ , and upon rearranging the governing Eqs. (9) to (12) and adding them, we obtain,

$$2 \left( 1 + \sum_{i=\beta,\gamma,\delta} \varepsilon_i \lambda_i^4 \right) T = Z_\alpha^2 + Z_\beta^2 \lambda_\beta^2 + Z_\gamma^2 \lambda_\gamma^2 + Z_\delta^2 \lambda_\delta^2. \quad (13)$$

Eq. (13) expresses that, in a system of interacting capillaries, the sum of the squares of the product of the non-dimensional radius with the non-dimensional distance invaded in all the capillaries is proportional to the invasion time  $T$ . For different arrangements of a system of 4 interacting capillaries having the same contrasts in capillary radii, the total capillary suction of the system remains the same. Therefore, for any of the  $4!/2 = 12$  possible arrangements, rearranging the equations governing the imbibition process, and adding them, leads to Eq. (13). However, the velocity at which the individual menisci travels in each of the tubes depends on the particular arrangement of the capillaries.

$z_\delta(t)$  relative to  $z_\beta(t)$  and  $z_\gamma(t)$  depends on the contrasts in the capillaries' radii.

The detailed development of the generalized one-dimensional model for this system of four interacting capillaries with arrangement  $\beta\gamma\alpha\delta$  is described in Appendix A. The pressure drop across each of the sections is determined individually, i.e., for sections (I)  $0 < z < z_\alpha$ , (II)  $z_\alpha < z < z_\beta$ , (III)  $z_\beta < z < z_\gamma$ , and (IV)  $z_\alpha < z < z_\delta$ . As spontaneous imbibition is driven by capillary forces, the sum of the pressure drops across all the sections of a capillary is equal to the capillary pressure of that capillary.

$$Pc_i = \left( \sum_j P_{i(j)} \right), \quad (3)$$

where  $P_{i(j)}$  is the pressure drop across the section of index  $j = (I), (II), (III), (IV)$  of the capillary of index  $i = \alpha, \beta, \gamma, \delta$ . By solving the system of equations expressing (i) Darcy's law in each of the capillaries, and (ii) the relations between the menisci's advancement and the fluid velocities and fluid exchange between the capillaries, we obtain the equations governing the flow in the interacting capillaries, which are,

$$Pc_\alpha = \frac{8\mu z_\alpha(t)}{r_\alpha^4 + r_\beta^4 + r_\gamma^4 + r_\delta^4} \left( r_\alpha^2 \frac{dz_\alpha}{dt} + r_\beta^2 \frac{dz_\beta}{dt} + r_\gamma^2 \frac{dz_\gamma}{dt} + r_\delta^2 \frac{dz_\delta}{dt} \right), \quad (4)$$

### C. Generalizing the one-dimensional spontaneous imbibition model in the interacting capillary system

Equation (13) is readily generalized to a system of  $n$  interacting capillaries, in the form

$$2 \left( \sum_{i=1}^n \varepsilon_i \lambda_i^4 \right) T = \sum_{i=1}^n \psi_i Z_i \quad (14)$$

where  $\psi_i = \pi r_i^2 z_i / (\pi r_\alpha^2 L)$  ( $j = 1, 2, \dots, n$ ) is the non-dimensional volume imbibed in the capillary of index  $j$ . Eq. (14) expresses that the sum over all capillaries of the non-dimensional volumes times the corresponding non-dimensional imbibition lengths, is proportional to time. This can be compared to the dynamics in a bundle of non-interacting capillaries, for which we know that the dynamics are diffusive, i.e., for each of the capillaries, the imbibed length square is proportional to time.

We note from the derivation of Eq. (13) for the system consisting of four capillaries, that each arrangement of the capillaries will have a different set of governing equations for menisci positions with time. This is because the knowledge of the arrangement is required to determine the regions of the capillaries across which the pressure equilibrates and the locations of fluid transfers. Therefore, for a system of  $n$  interacting capillaries, we now propose an algorithm which can determine the imbibition behaviour in the bundle of interacting capillaries and form the governing equations for a generalized model of such systems of  $n$  interacting capillaries. A MATLAB program has been written to implement this algorithm and obtain the advancement of the menisci,  $z_l(t)$ , where  $l = 1, 2, 3, \dots, n$ , as a function of time. The step-by-step procedure is described in detail in Appendix B, but its principles can be described in the following manner.

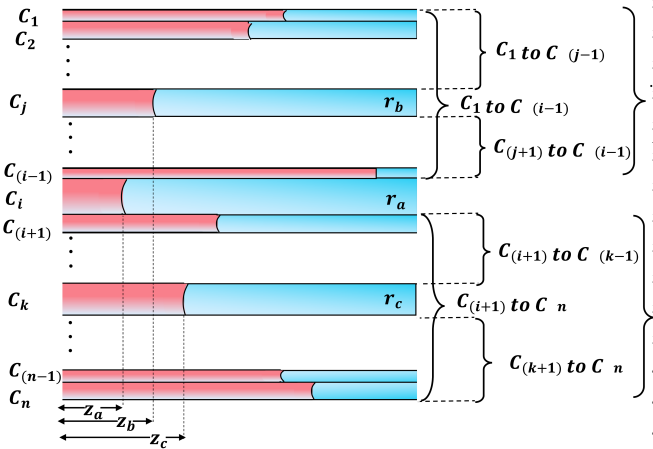


FIG. 4. Schematic of spontaneous imbibition in an  $n$ -capillary system where the capillaries are positioned randomly. The capillaries in the arrangement are denoted by  $C_1, C_2, \dots, C_n$ . The capillary radii are denoted as  $r_a, r_b, r_c, \dots$ , and the corresponding imbibition distances at time  $t$  are denoted by  $z_a(t), z_b(t), z_c(t), \dots$ .

First, the algorithm searches for the capillary of largest radius in the arbitrary arrangement, whose meniscus position is

$z_a$  at a given time; it is denoted  $C_i$  in Fig. 4, where the capillaries in the order of arrangement are denoted from  $C_1$  to  $C_n$ . The pressure drop in the region  $0 < z < z_a$  is determined for all the capillaries and the algorithm then considers two regions: the ‘top region’ consisting of the capillaries  $C_1$  to  $C_{(i-1)}$  and the ‘bottom region’ consisting of the capillaries  $C_{(i+1)}$  to  $C_n$  (see Fig. 4). The largest radius capillaries in each of these two regions are determined and the pressure drop in the respective regions are determined for sections  $z_a < z < z_b$  and  $z_a < z < z_c$ . Now, each of these two regions is further divided into two subregions each, i.e., containing the capillaries  $C_1$  to  $C_{(j-1)}$  on the one hand and  $C_{(j+1)}$  to  $C_{(i-1)}$  on the other hand in the ‘top region’, and  $C_{(i+1)}$  to  $C_{(k-1)}$  on the one hand and  $C_{(k+1)}$  to  $C_n$  on the other hand in the ‘bottom region’. The pressure drops are determined in each of the subregions. This procedure is then performed recursively until the algorithm has identified the pressure drop in each of the sections for every capillary. It can then formulate the governing equations, which are consequently solved to obtain the advancement of all menisci as a function of time.

### III. RESULTS AND DISCUSSIONS

We first explore the imbibition of a system of four interacting capillaries, followed by the imbibition in a system consisting of 20 capillaries.

#### A. Interacting four-capillary system

In section II A, we have anticipated that, in an ordered arrangement, the meniscus in the capillary of smallest radius,  $\delta$ , will always lead, followed by the capillary of second smallest radius,  $\gamma$ , as shown in Fig. 2, while the meniscus in the capillary  $\alpha$  always lags behind. Solving the governing equations for this arrangement, we always get the same trend, i.e.,  $z_\alpha(t) < z_\beta(t) < z_\gamma(t) < z_\delta(t)$  for the imbibed lengths in the capillaries at any given time during the imbibition process. However,  $4!/2 = 12$  arrangements are possible for an interacting four-capillary system, for any given 4 radii of the capillaries. In section II B we chose one arrangement  $\beta\gamma\alpha\delta$  and anticipated 3 cases of different relative positioning of menisci. The possibility of occurrence of these 3 cases depends upon the radii contrast in the capillaries. A change in radii contrast changes the pressure fields in the capillaries, which governs the menisci positions. Each of the 3 cases shown in Fig. 3 are shown in Fig. 5 (a), (c), (e). Solving Eqs. (9) to (12) over non-dimensional times, we show in Fig. 5 (b), (d), (f), how the relative positions of the plots of  $Z_\beta, Z_\gamma, Z_\delta$  as a function of time change when the contrast in the radii of capillaries are changed according to the three configurations addressed in Fig. 5 (a), (c), (e).

We now consider two other random arrangements  $\gamma\delta\alpha\beta$  and  $\gamma\alpha\beta\delta$ , which are illustrated in Figs. 6 and 7, respectively. In these figures, we show the schematic of the menisci locations at a given time during imbibition in (a), (c), (e). The corresponding time evolution of the positions of menisci in

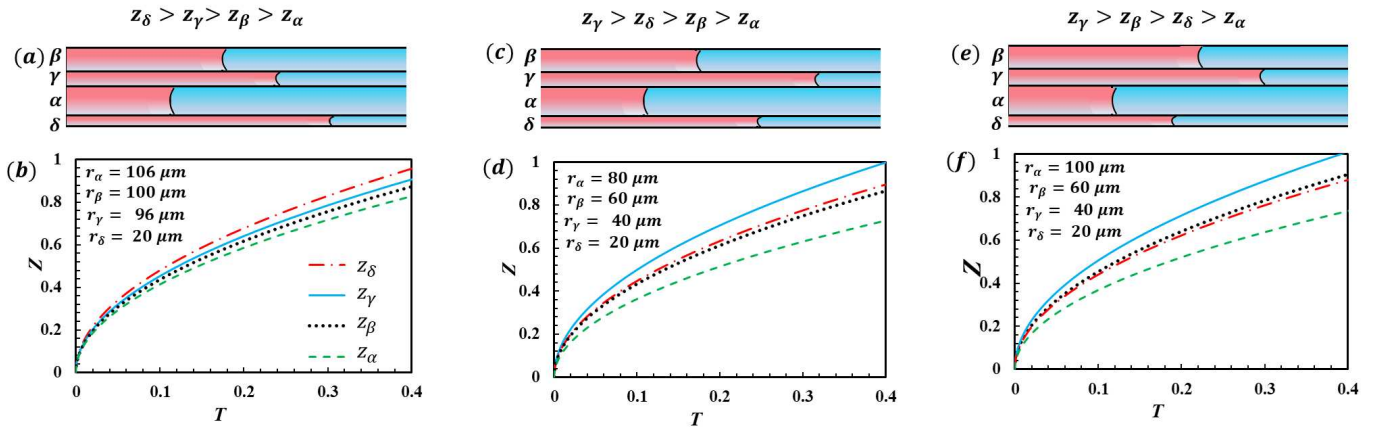


FIG. 5. Spontaneous imbibition in a system of four interacting capillaries which are positioned with respect to each other according to the arrangement  $\beta\gamma\alpha\delta$ , for three different contrasts in capillary radii. (a), (c), (e) represent the schematics of possible imbibition behavior at a given time  $t$ . The distribution of radii predicting the imbibition phenomenon are indicated in the plots (b), (d) and (f). The non-dimensional times at which the leading meniscus reaches the outlet end of the interacting capillary system ( $T_{bt}$ ) for the cases (b), (d) and (f) are 0.43, 0.40 and 0.39, respectively.

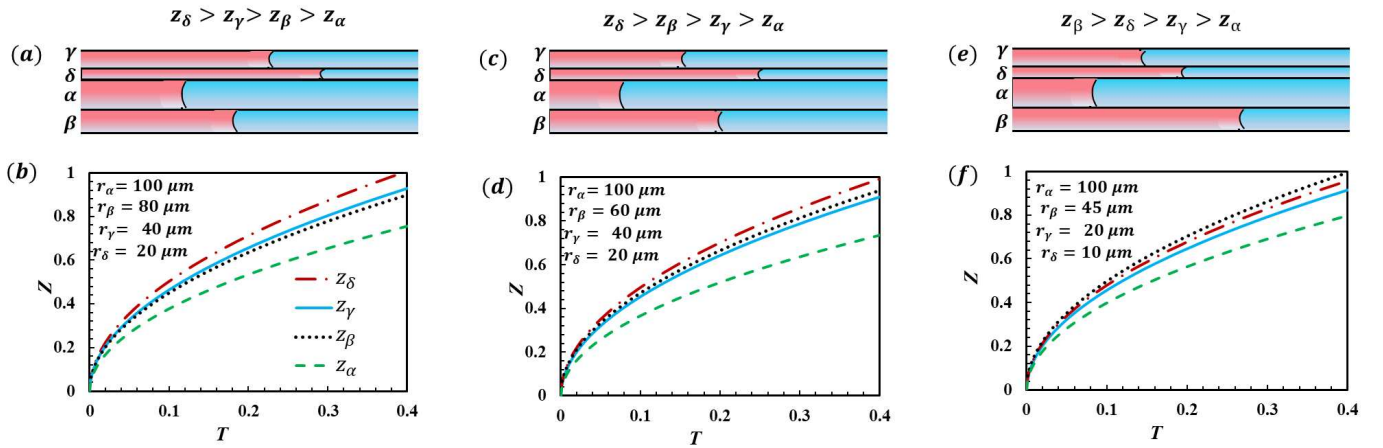


FIG. 6. Spontaneous imbibition in a system of four interacting capillaries, spatially arranged as  $\gamma\delta\alpha\beta$ . Depending upon the contrasts in capillary radii, at a given time, the relative positions of the menisci vary. (a), (c), (e) represent the schematics of possible imbibition behavior. The non-dimensional meniscus positions and the radii contrasts corresponding to the schematics of (a), (c), (e) are shown in (b), (d), (f) respectively, as a function of the non-dimensional time. The times at which the invading fluid reaches the outlet end ( $T_{bt}$ ) for the cases (b), (d) and (f) are 0.38, 0.40 and 0.39, respectively.

414 the four capillaries are shown in (b),(d),(f). Each of these fig-430  
 415 ures shows that the contrast in the capillary radii, for a given-431  
 416 arrangement, impacts the relative positions of the menisci at-432  
 418 any given time. Conversely, in Figs. 5(f), 6(d), and 7(b), the-433  
 419 radii of the capillaries in the interacting capillary system are-434  
 420 identical but the arrangements of the capillaries are different-435  
 421 For the arrangement  $\beta\gamma\alpha\delta$  shown in Fig. 5(f), the menisci-436  
 422 positions are ordered according to  $Z_\gamma > Z_\beta > Z_\delta > Z_\alpha$  while-437  
 423 for the arrangement  $\gamma\delta\alpha\beta$  shown in Fig. 6(d) the menisci posi-438  
 424 tions are ordered according to  $Z_\delta > Z_\beta > Z_\gamma > Z_\alpha$  and for-439  
 425 the arrangement  $\alpha\beta\gamma\delta$  shown in Fig. 7(b), the menisci posi-439  
 426 tions are ordered according to  $Z_\delta > Z_\gamma > Z_\beta > Z_\alpha$ . Hence-440  
 427 for an interacting multi-capillary system, both the contrasts-441  
 428 in capillary radii and their arrangement are crucial in deter-442  
 429 mining the imbibition behavior. The non-dimensional time at-443

which the imbibing fluid first breaks through or reaches the non-dimensional length 1 in one of the interacting capillaries, and the radius of the capillary through which the breakthrough occurs, are impacted accordingly, as reported in the captions of Fig. 5, 6 and 7. Note that in Figs. 5, 6, 7, the schematics presented in (a), (c) and (e) are not necessarily to scale, either for the capillaries' radii (indicated in the legends of (b), (d) and (f)) or for the imbibition lengths.

We further illustrate the imbibition phenomenon in a system of four interacting capillaries for three arrangements out of the 12 possible arrangements in Fig. 8. The radii of the capillaries are  $r_\alpha = 80$  m,  $r_\beta = 60$  m,  $r_\gamma = 40$  m, and  $r_\delta = 20$  m for all the arrangements. In Fig. 8(a), where the capillaries are in the ordered arrangement ( $\alpha\beta\gamma\delta$ ), the leading meniscus is in the capillary with the smallest radius ( $\delta$ ). For the

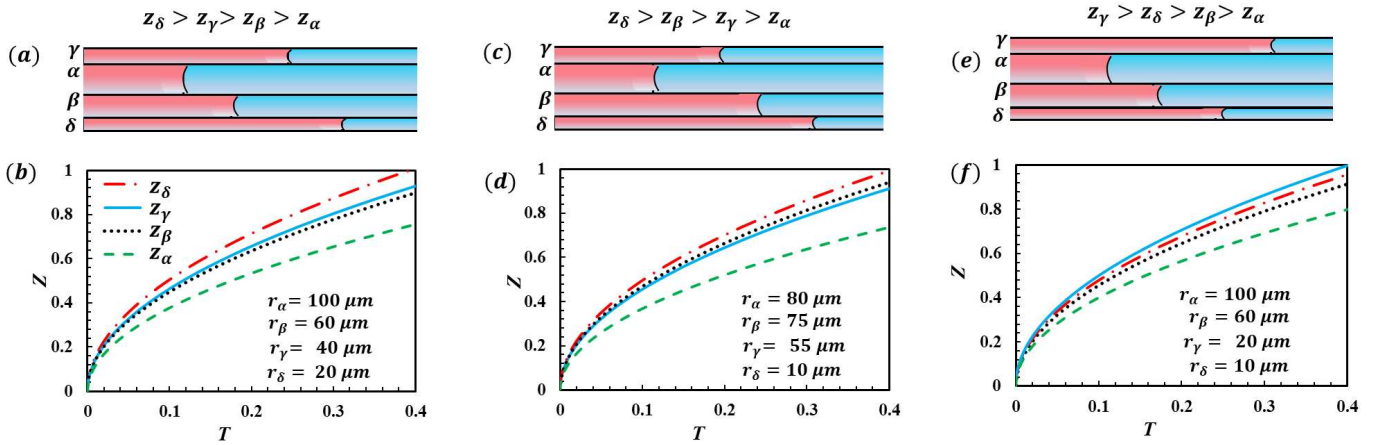


FIG. 7. Spontaneous imbibition in a system of four interacting capillaries, spatially arranged as  $\gamma\alpha\beta\delta$ . Depending upon the contrasts in capillary radii, at a given time, the relative positions of the menisci vary. (a), (c), (e) represent the schematics of possible imbibition behavior. The non-dimensional meniscus positions and the radii contrasts corresponding to the schematics of (a), (c), (e) are shown in (b), (d), (f) respectively, as a function of the non-dimensional time. The times ( $T_{bt}$ ) at which the invading fluid first reaches the outlet in any of the capillaries are 0.38, 0.42 and 0.38 for the cases (b), (d) and (f), respectively.

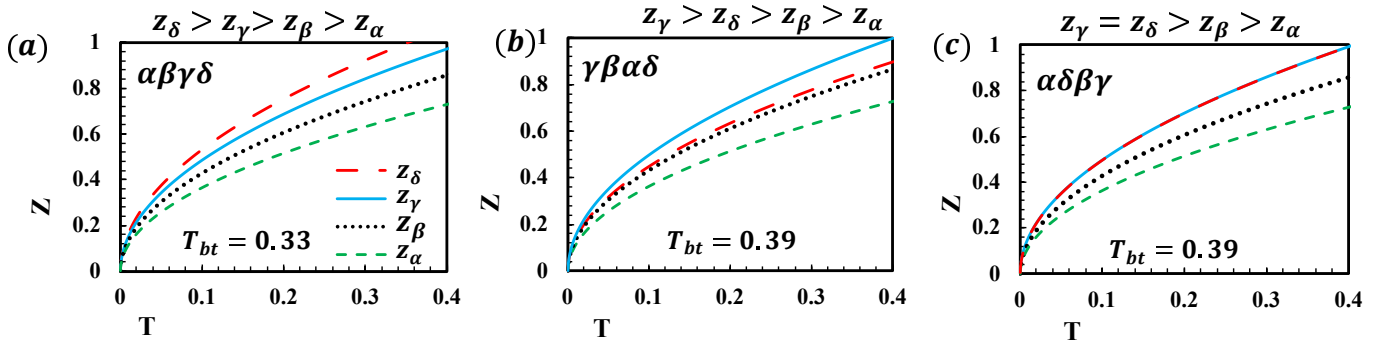


FIG. 8. Spontaneous imbibition in a system of four interacting capillaries of radii  $r_\alpha = 80$  m,  $r_\beta = 60$  m,  $r_\gamma = 40$  m and  $r_\delta = 20$  m. The non-dimensional positions of the four menisci are shown as functions of the non-dimensional time for three of the 12 possible arrangements (a)  $\alpha\beta\gamma\delta$ , (b)  $\gamma\beta\alpha\delta$ , and (c)  $\alpha\delta\beta\gamma$  are shown. The relative position of the menisci with time and the breakthrough time depend upon the arrangement of the capillaries, for a given contrast in the radii.

445 same contrast in radii and the arrangement  $\gamma\beta\alpha\delta$  (Fig. 8(b)),<sup>464</sup>  
 446 the leading meniscus is in capillary  $\gamma$ . For arrangement  $\alpha\delta\beta\gamma$ <sup>465</sup>  
 447 shown in Fig. 8(c), the menisci in capillaries  $\gamma$  and  $\delta$  travel  
 448 at the same velocity at all times. It can also be observed  
 449 from Fig. 8 that the breakthrough times change with the ar-<sup>466</sup>  
 450 rangement of the capillaries; while the breakthrough for the  
 451 ordered arrangement (Fig. 8(a)) occurs at  $T = 0.33$ , for the  
 452 other two other arrangements shown in Fig. 8(b) and (c), the<sup>467</sup>  
 453 breakthrough occurs at  $T = 0.40$ . Similar plots are shown for<sup>468</sup>  
 454 all 12 possible arrangements in Fig. C.1 of Appendix C; all<sup>469</sup>  
 455 the arrangements are found to have breakthrough times in the<sup>470</sup>  
 456 range  $T = 0.33$  to  $T = 0.40$ . For a wetting fluid of viscos-<sup>471</sup>  
 457 ity  $10^{-3}$  Pa·s and surface tension of  $73 \times 10^{-3}$  N/m impreg-<sup>472</sup>  
 458 nating the empty capillary system of length 1 m and with a<sup>473</sup>  
 459 maximum capillary radius of 80 m, the non-dimensional time<sup>474</sup>  
 460 corresponding to  $T = 0.01$  is 6.84 s, so the breakthrough for<sup>475</sup>  
 461 the arrangements shown in Fig. 8 occurs between 225.7 s and<sup>476</sup>  
 462 273.6 s. Hence, for the four-capillary system, we can summa-<sup>477</sup>  
 463 rize that the arrangement of the capillaries and the contrasts in<sup>478</sup>  
 479

capillary radii significantly affect the breakthrough time and the index of the capillary through which breakthrough occurs.

## B. System consisting of 20 interacting capillaries

From the above analysis, we see that for any interacting multi-capillary system, the capillary having the leading meniscus and the breakthrough time both depend on the contrast in the capillary radii and on the spatial arrangement of capillaries. We now use the generalized model to predict imbibition in a system consisting of  $n = 20$  interacting capillaries, focusing on the impact of the arrangement. We assume no spatial correlations in the capillaries' radii. The number of different arrangements for  $n = 20$  is  $20! / 2 = 1.216 \times 10^{18}$ . We run the generalized model on 1000 random arrangements for capillaries whose radius distribution is uniform between 10 m (minimum radius) and 200 m (maximum radius).

We show in Fig. 9(a), the imbibition length in the capillar-

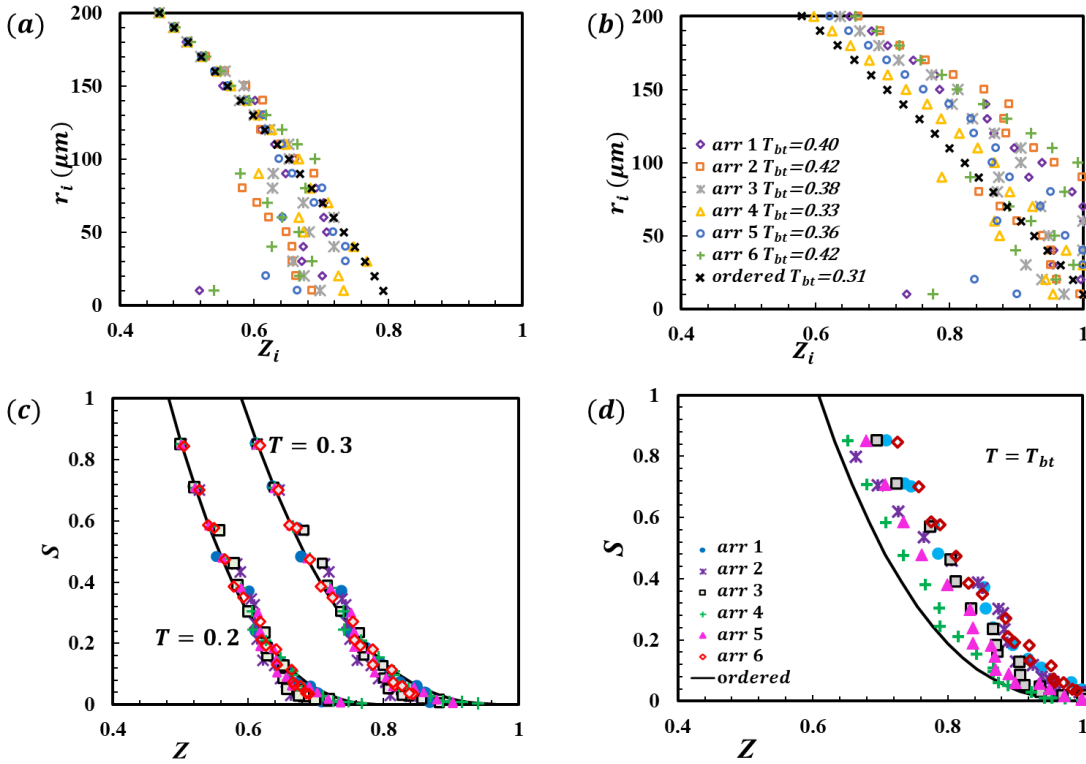


FIG. 9. Spontaneous imbibition in 7 systems of twenty interacting capillaries with identical radii but different spatial arrangements: 6 random arrangements and one ordered arrangement. (a) radii vs. imbibition length at  $T = 0.2$ ; (b) radii vs. imbibition length at breakthrough time,  $T = T_{bt}$ . (c) saturation vs. longitudinal position at  $T = 0.2$  and  $T = 0.3$ , (d) saturation vs. longitudinal position at breakthrough time,  $T = T_{bt}$ .

ies vs the radii of the capillaries at the non-dimensional time  $T = 0.2$  for 6 random arrangements (denoted  $arr1$ ,  $arr2$ ,  $arr3$ ,  $arr4$ ,  $arr5$  and  $arr6$  in the figure), and the ordered arrangement (denoted  $ordered$  in the figure). We have chosen the 6 random arrangements such that the disparity in the breakthrough time and the capillary radius through which the breakthrough occurs can be observed for the given radii contrast of the capillaries. We see from Fig. 9(a) that, at  $T = 0.2$ , the capillary having the leading meniscus is different for different arrangements and the menisci positions in the capillaries are also dependent on the arrangement. For instance, at  $T = 0.2$  the meniscus in the capillary of radius 10  $\mu\text{m}$  (smallest radius) has traveled a non-dimensional length of 0.79 for the ordered arrangement, whereas for random arrangement number 1, the non-dimensional length invaded in the smallest capillary is 0.51. In Fig. 9(b), we illustrate the relationship between the radii and the imbibition length in all capillaries at breakthrough time. The breakthrough time for different arrangements is given in the legend of the arrangement in Fig. 9(b). Breakthrough in the systems of 20 interacting capillaries occurs through different capillaries and at different times for the 6 random arrangements and the ordered arrangement.

The saturation at a given imbibition length  $Z$  can be defined as the ratio of the cross-sectional area occupied by the imbibing fluid at  $Z$  to the total cross-sectional area of the capillary system, i.e.,  $(\sum_{j=1}^{n_f} r_j^2) / \sum_{i=1}^n r_i^2$ , where  $n_f(Z)$  is the number of capillaries filled by the imbibing fluid at  $Z$ , and the indices  $j$  refer to all such capillaries. The plot of saturation vs. longi-

tudinal position is shown in Fig. 9(c) at  $T = 0.2$  and  $T = 0.3$ , for all the 7 spatial arrangements. These saturation profiles of the interacting capillary system depend significantly on the arrangement of the capillaries. For example, at  $T = 0.3$ , the saturation at  $Z = 0.7$  is 0.43 for the random arrangement number 3, and 0.35 for the ordered arrangement as indicated in Fig. 9(c).

In Fig. 9(d) we show how saturation varies with the longitudinal position at breakthrough time for the 7 arrangements. The amount of non-wetting fluid displaced at the time of breakthrough is different between the different arrangements. We also observe from Fig. 9(a) that the random arrangements where the leading meniscus is in a capillary of larger radius, will have a longer breakthrough time as shown in Fig. 9(b). This will also cause the saturation of the random arrangement to be larger at the breakthrough time, which can be observed in Fig. 9(d).

However, since the contrast in the radii of the capillaries is identical for all arrangements, the effective capillary suction causing the imbibition phenomenon is also identical in all cases. Therefore, at a given time  $T$ , the global wetting fluid saturation in the interacting capillary system will be the same for all arrangements, which is determined as  $S = \sum_{i=1}^n r_i^2 Z_i / \sum_{i=1}^n r_i^2$ . The fraction of the interacting capillary system occupied with the imbibing phase at  $T = 0.2$  is 0.55 and at  $T = 0.3$ ,  $S$  is 0.67 for all the 7 arrangements. But this is only applicable until breakthrough occurs in one of the arrangements.

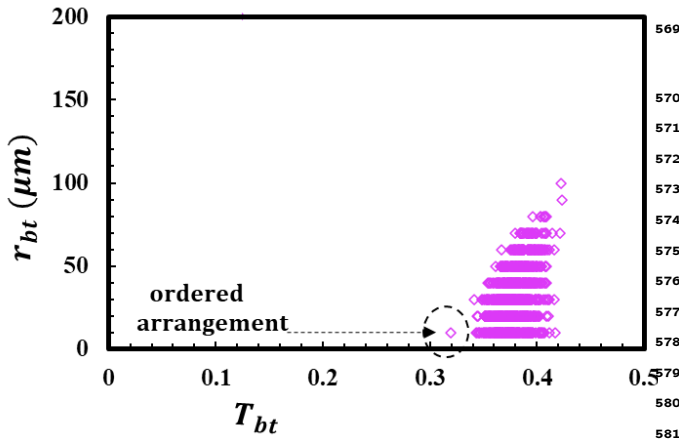


FIG. 10. Radii of the capillaries in which breakthrough occurs vs. breakthrough time in 1000 randomly-chosen arrangements of a system of 20 interacting capillaries with radii uniformly distributed between 10 and 200 m (the upper boundary of the vertical scale is thus chosen to 200 m). The shortest breakthrough time is observed in the ordered arrangement, at  $T = 0.31$ , and the maximum observed breakthrough time is  $T = 0.42$ . The largest radius of a capillary through which breakthrough occurs is 100 m while the smallest one is 10 m.

## C. Discussion

We now compare the predictions of our analytical model of interacting capillaries to those of the standard capillary bundle model, and discuss how the predictions of our model compare to experimental measurements in quasi-2D porous media. We use our model within a stochastic approach, that is, for a given number  $n$  of capillaries of known radii we consider the average behavior of all  $m = n! / 2$  different spatial arrangements of the capillaries. When  $m$  is too large to be tractable even for our very fast semi-analytical model (for example for  $n = 20$ ,  $m > 1.21 \cdot 10^{18}$ ), we consider the average behavior of a sufficiently large subsample of  $R < m$  randomly-chosen spatial arrangements.

### 1. Confronting predictions from the classic (non-interacting) capillary bundle to our model

We show the spatial saturation profile for the classic capillary bundle model with  $n = 20$  capillaries at three different times ( $T = 0.1$ ,  $T = 0.3$  and  $T = T_{bt} = 0.5$ ) in Fig 11(a), and the average spatial saturation profile for 1000 randomly-chosen different spatial arrangements, for a system of 20 interacting capillaries (as predicted by our model) at the same three times in Fig 11(b). Note that the number of spatial arrangements was chosen after a convergence study which we present in Appendix D (see in particular Fig. D.1).

The capillary radii are identical in the two cases. For non-interacting capillaries, by non dimensionalizing the Washburn's law,  $z_i^2 = (Pc_i r_i^2 / 4\mu)t$ , we obtain

$$Z_i^2 = 2\varepsilon_i \lambda_i^2 T, \quad (15)$$

where  $Z_i = z_i / L$  is the non-dimensional length imbibed in the capillary of radius  $r_i$  and  $L$  is the total length of the capillary system. The time is non-dimensionalised as  $T = t(Pc_\alpha r_\alpha^2) / (8\mu L^2)$ . In Eq. (15),  $\varepsilon = Pc_i / Pc_\alpha$  and  $\lambda_i = r_i / r_\alpha$ , where  $Pc_\alpha$  and  $r_\alpha$  are respectively the capillary pressure and radius of the widest capillary (200 m). The maximum value of  $\varepsilon_i$  and  $\lambda_i$  are 1, which occurs for the largest radius capillary. For all other capillaries  $\varepsilon_i$  and  $\lambda_i$  are always smaller than 1.

As discussed previously, in the classic capillary bundle model, imbibition follows Washburn's diffusive dynamics and therefore the invaded length is the largest in the capillary of largest radius. As illustrated in Fig. 11(a), due to the large cross-section area of that widest capillary, it contributes to a large fraction of the cross-sectional saturation for the bundle-of tubes model. On the contrary, in our interacting-capillary system, the largest radius capillary always has the least advanced meniscus, at any time. Consequently, the breakthrough time for the capillary bundle model is 136.5 s (at  $T = 0.5$ ), at which the fractional volume occupied by the invading fluid is 0.86. This is considerably larger than the breakthrough time for interacting capillary systems, which occurs between 84.63 s and 114.66 s (between  $T = 0.31$  and  $T = 0.42$ ), depending on the configuration, and the fractional volumes occupied by the imbibing fluid across the 1000 arrangements lie between 0.69 and 0.79. In Fig. 11(b), we show

In Fig. 10 we have plotted the radius of the capillary having the leading meniscus vs. the breakthrough time for the 1000 randomly chosen arrangements, assumed to be representative of the entire statistics. We see that when a wetting fluid of viscosity of  $10^{-3}$  Pa·s and surface tension of  $73 \times 10^{-3}$  N/m imbibes a twenty-capillary system of length 1 m and maximum capillary radius of 200 m, the non-dimensional time of  $T = 0.01$  corresponds to 2.73 s. If such a wetting fluid were considered to imbibe into this interacting capillary system, the breakthrough which occurs between  $T = 0.31$  and  $T = 0.42$  corresponds to the dimensional times of 84.63 s and 114.66 s. Therefore, for the same contrast in capillary radii, the maximum and minimum breakthrough time are approximately 30 s apart, indicating that the breakthrough time significantly depends on the arrangement of the capillaries. It can also be observed from Fig. 10 that breakthrough in an ordered multi-capillary system occurs through the capillary of smallest radius at  $T = 0.31$ , which is the smallest breakthrough time compared to other arrangements. Fig 10 also shows that the largest radius of a capillary through which breakthrough occurs is as large as 100 m, while the minimum radius of the capillary through which breakthrough occurs is 10 m. For arrangement number 6 (+ symbols), the leading meniscus is in the 100 m radius capillary and breakthrough occurs at  $T_{bt} = 0.42$  as shown in Fig. 9(b). From Fig. 10, we also see that, when breakthrough occurs through the smallest radius capillary, the breakthrough time may vary between  $T = 0.31$  and  $T = 0.41$ , and the total volume fraction of the interacting capillary system occupied by the invading phase can lie between 0.69 and 0.79. In contrast, if breakthrough occurs through the capillary of radius 70 m, the breakthrough time lies between  $T = 0.38$  and  $T = 0.42$  and the total volume fraction imbibed by the wetting phase lies between 0.76 and 0.8.

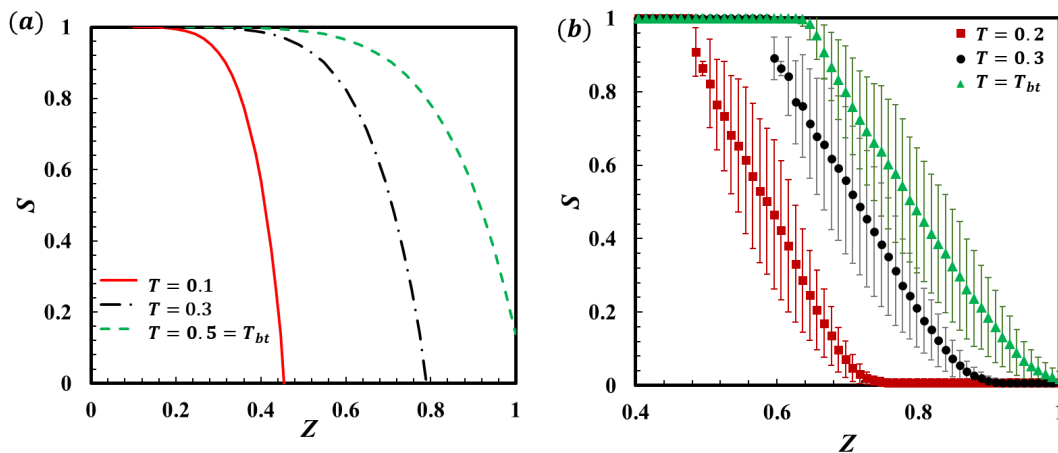


FIG. 11. (a) Spatial saturation profile during spontaneous imbibition in a bundle-of-tubes consisting of twenty non-interacting capillaries at  $T = 0.1$ ,  $T = 0.3$ , and  $T = T_{bt} = 0.5$ . (b) Average spatial saturation profile for 1000 different spatial arrangements of the system consisting of twenty interacting capillaries of identical radii as in (a), at  $T = 0.1$ ,  $T = 0.3$ ,  $T = T_{bt}$ .

621 the averaged saturation values along the length of the capil-655  
 622 lary system for all the 1000 arrangements of the twenty in-656  
 623 teracting capillary system at non-dimensional times  $T = 0.1$ ,  
 624 0.2 and at breakthrough, i.e.,  $T_{bt}$ . We see from fig. 11(b) that-657  
 625 the standard deviation across the arrangements is due to the-658  
 626 difference in the relative positioning of the menisci resulting-659  
 627 from the spatial arrangement of the capillaries. 660

## 2. Confronting predictions from the model to experimental measurements from previous studies

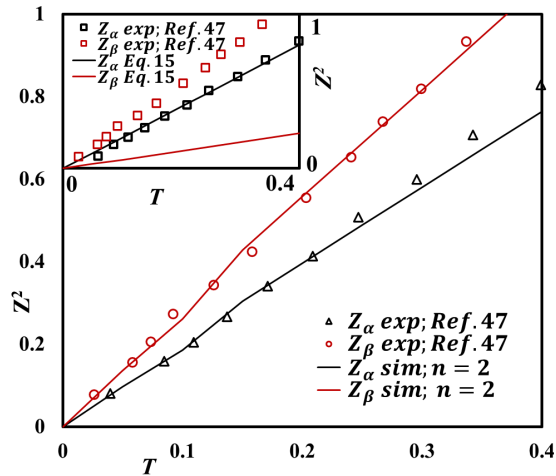
661 The spatial profiles of saturation for the interacting multi-  
 662 capillary system are consistent with observations of imbibition  
 663 phenomena in quasi-2D porous media described by Dong  
 664 et al., Ding et al., Debbabi et al., and Akbari et al.,<sup>48,66–68</sup>.  
 In real porous media, the imbibing fluid saturation decreases  
 gradually with longitudinal position, similarly to the trend  
 shown by the interacting multi-capillary system. It was also  
 previously described that the lagging macroscopic front is  
 mostly responsible for the saturation of a porous medium<sup>47</sup>,  
 which is in good agreement with the saturation profile ant-  
 icipated by the interacting multi-capillary system, as shown  
 in Fig. 11(b). The saturation profile for the (classic) non-  
 interacting capillary bundle (Fig. 11a) predicts that the large  
 pores are responsible for the leading macroscopic front and  
 the saturation of the porous medium, which is contrary to the  
 interacting capillaries model (shown in Fig. 11(a)) and the  
 experimental observations in real porous media.<sup>47,54,62,69,70</sup>

Furthermore, in the following we compare the predictions  
 of our model to two data sets from the literature, both taken  
 from Ref.<sup>47</sup>.

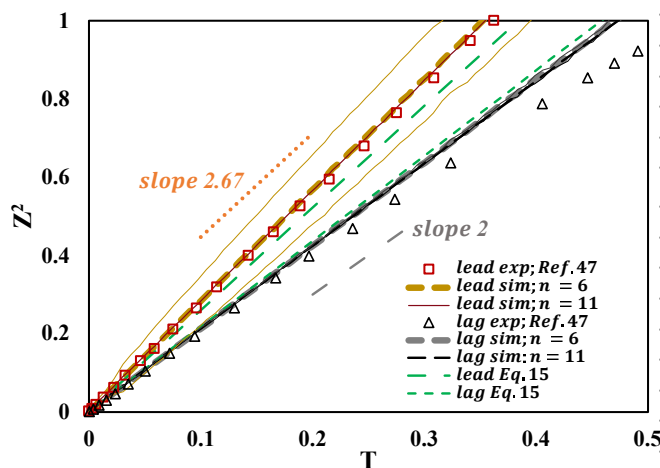
a. *Two capillary system:* We first compare our model  
 predictions to measurements performed on a system of two  
 capillaries consisting of a thread positioned inside a cylindri-  
 cal tube. The time evolution of the menisci position squared,  
 as predicted by our model, compares well with the experi-  
 mental observations for both capillaries (Fig. 12). The radi-  
 us of the large capillary was  $r_\alpha = 300$  m, that of the  
 thread  $r_\beta = 170$  m. From the experimental data<sup>47</sup>, the value  
 of  $(Pc_\alpha r_\alpha^2)/(8\mu L^2)$  is  $0.0108$  s<sup>-1</sup>, which is used to non-  
 dimensionalize time in Fig. 12. The predictions from the clas-  
 sic (non-interacting) capillary bundle model (Eq. 15) are also  
 shown in the inset of Fig. 12 for comparison. The imbibition  
 in the wider capillary is little impacted by the imbibition in  
 the (much) narrower capillary, so that the prediction of the non-  
 interacting capillary bundle for the wider capillary are similar

628 For instance, the leading meniscus for an orderly arrange-665  
 629 ment of interacting capillary system is in the smallest radius capillary-666  
 630 and we know that the fraction of saturation contributed by-667  
 631 the smallest radius capillary is small. For the arrangement-668  
 632 2 shown in Fig. 9, the leading meniscus is in the capillary-669  
 633 of radius 100 m. In the capillary bundle model, the cross-670  
 634 section area of the leading capillary (200m) is 13.93% of the-671  
 635 total cross-section area, whereas for the ordered arrangement-672  
 636 and the arrangement number 2, the respective cross-section-673  
 637 area of the leading meniscus capillaries are 0.03% and 3.43%-674  
 638 Consequently, as shown by Fig. 11(b), the cross-sectional sat-675  
 639 uration decreases gradually with longitudinal position for the-676  
 640 classic capillary bundle model, while in the case of interact-677  
 641 ing capillaries a steep decrease is observed already at small-678  
 642 longitudinal positions. Fig. 11(b) also shows that the standar-679  
 643 deviation in saturation from the average across the 1000 ar-680  
 644 rangements at  $T = 0.1$  and  $T = 0.2$ , which is as high as 0.2-681  
 645 at  $Z = 0.59$  and  $0.69$ , respectively; whereas for  $T = T_{bt}$ , it-682  
 646 is 0.18 at  $Z = 0.76$ . In real two-dimensional porous medi-683  
 647 where the spatial arrangement of pores may vary, the interact-684  
 648 ing capillaries model will be more helpful in predicting the ac-685  
 649 curate imbibition behaviour than the classic capillary bundle-686  
 650 model. The saturation of the porous medium with length and-687  
 651 the breakthrough time significantly differ for the classic (non-688  
 652 interacting) capillary bundle and for the different arrangements-689  
 653 of the interacting multi-capillary system, although the contrast-690  
 654 in the radii of the capillaries is the same. 691

692 to the experimental data; however the non-interacting capil-699  
693 lary bundle underestimates the advancement of the meniscus700  
694 in the narrower capillary (the thread) by a factor 5.



695  
696  
719 FIG. 12. Imbibition in a system of two interacting capillaries hav-  
720 ing radii  $r_\alpha = 300$  m and  $r_\beta = 170$  m. Predictions from our semi-  
721 analytical model (solid lines) compare well to the data (symbols) of  
722 Bico and Quéré<sup>47</sup>. The inset of the figure shows the same compar-  
723 ison for predictions of the classic (non-interacting) capillary bundle,  
724 obtained through Eq. 15, which underestimates  
725 the advancement  $Z_\beta$  of the meniscus in the narrower capillary (red  
726 line) by a factor 5.



727  
728  
729  
730  
731  
732  
733  
734  
735  
736  
737  
738  
739  
740  
741  
742  
743  
744 FIG. 13. Dependence of the square of the non-dimensional imbibition  
745 length on non-dimensional time. The experimental findings of  
746 Bico and Quéré<sup>47</sup> are shown with red squares (for leading front) and  
747 black triangles (for lagging front). The predictions of our model for  
748 two different samplings (6 and 12 interacting capillaries) of the uni-  
749 form pore size distribution are shown with lines, respectively orange  
750 and dashed (for  $n = 6$ ) or purple and solid (for  $n = 11$ ) for the leading  
751 front, and thick, gray and dashed (for  $n = 6$ ) or black and dashed for  
752 the lagging front. The results from the classic, non-interacting capil-  
753 lary bundle are presented for comparison for the leading front (green  
754 long-dashed line) and lagging fronts (green dashed line).

701  
702  
703  
704  
705  
706  
707  
708  
709  
710  
711  
712  
713  
714  
715  
716  
717  
718  
719  
720  
721  
722  
723  
724  
725  
726  
727  
728  
729  
730  
731  
732  
733  
734  
735  
736  
737  
738  
739  
740  
741  
742  
743  
744  
745  
746  
747  
748  
749  
750  
751  
752  
753  
754  
755  
756  
757  
758  
759  
760  
761  
762  
763  
764  
765  
766  
767  
768  
769  
770  
771  
772  
773  
774  
775  
776  
777  
778  
779  
780  
781  
782  
783  
784  
785  
786  
787  
788  
789  
790  
791  
792  
793  
794  
795  
796  
797  
798  
799  
800  
801  
802  
803  
804  
805  
806  
807  
808  
809  
810  
811  
812  
813  
814  
815  
816  
817  
818  
819  
820  
821  
822  
823  
824  
825  
826  
827  
828  
829  
830  
831  
832  
833  
834  
835  
836  
837  
838  
839  
840  
841  
842  
843  
844  
845  
846  
847  
848  
849  
850  
851  
852  
853  
854  
855  
856  
857  
858  
859  
860  
861  
862  
863  
864  
865  
866  
867  
868  
869  
870  
871  
872  
873  
874  
875  
876  
877  
878  
879  
880  
881  
882  
883  
884  
885  
886  
887  
888  
889  
890  
891  
892  
893  
894  
895  
896  
897  
898  
899  
900  
901  
902  
903  
904  
905  
906  
907  
908  
909  
910  
911  
912  
913  
914  
915  
916  
917  
918  
919  
920  
921  
922  
923  
924  
925  
926  
927  
928  
929  
930  
931  
932  
933  
934  
935  
936  
937  
938  
939  
940  
941  
942  
943  
944  
945  
946  
947  
948  
949  
950  
951  
952  
953  
954  
955  
956  
957  
958  
959  
960  
961  
962  
963  
964  
965  
966  
967  
968  
969  
970  
971  
972  
973  
974  
975  
976  
977  
978  
979  
980  
981  
982  
983  
984  
985  
986  
987  
988  
989  
990  
991  
992  
993  
994  
995  
996  
997  
998  
999  
1000

744  
745  
746  
747  
748  
749  
750  
751  
752  
753  
754  
755  
756  
757  
758  
759  
760  
761  
762  
763  
764  
765  
766  
767  
768  
769  
770  
771  
772  
773  
774  
775  
776  
777  
778  
779  
780  
781  
782  
783  
784  
785  
786  
787  
788  
789  
790  
791  
792  
793  
794  
795  
796  
797  
798  
799  
800  
801  
802  
803  
804  
805  
806  
807  
808  
809  
810  
811  
812  
813  
814  
815  
816  
817  
818  
819  
820  
821  
822  
823  
824  
825  
826  
827  
828  
829  
830  
831  
832  
833  
834  
835  
836  
837  
838  
839  
840  
841  
842  
843  
844  
845  
846  
847  
848  
849  
850  
851  
852  
853  
854  
855  
856  
857  
858  
859  
860  
861  
862  
863  
864  
865  
866  
867  
868  
869  
870  
871  
872  
873  
874  
875  
876  
877  
878  
879  
880  
881  
882  
883  
884  
885  
886  
887  
888  
889  
890  
891  
892  
893  
894  
895  
896  
897  
898  
899  
900  
901  
902  
903  
904  
905  
906  
907  
908  
909  
910  
911  
912  
913  
914  
915  
916  
917  
918  
919  
920  
921  
922  
923  
924  
925  
926  
927  
928  
929  
930  
931  
932  
933  
934  
935  
936  
937  
938  
939  
940  
941  
942  
943  
944  
945  
946  
947  
948  
949  
950  
951  
952  
953  
954  
955  
956  
957  
958  
959  
960  
961  
962  
963  
964  
965  
966  
967  
968  
969  
970  
971  
972  
973  
974  
975  
976  
977  
978  
979  
980  
981  
982  
983  
984  
985  
986  
987  
988  
989  
990  
991  
992  
993  
994  
995  
996  
997  
998  
999  
1000

919  
920  
921  
922  
923  
924  
925  
926  
927  
928  
929  
930  
931  
932  
933  
934  
935  
936  
937  
938  
939  
940  
941  
942  
943  
944  
945  
946  
947  
948  
949  
950  
951  
952  
953  
954  
955  
956  
957  
958  
959  
960  
961  
962  
963  
964  
965  
966  
967  
968  
969  
970  
971  
972  
973  
974  
975  
976  
977  
978  
979  
980  
981  
982  
983  
984  
985  
986  
987  
988  
989  
990  
991  
992  
993  
994  
995  
996  
997  
998  
999  
1000

697  
698  
999  
1000

the porous medium's length, with a pressure gradient that is  
 $P_{c\text{eff}}/z$ ,  $P_{c\text{eff}}$  being a constant effective capillary pressure de-  
 fined for the entire medium. Then the Darcy law reads

$$\frac{dz}{dt} = \frac{K P_{c\text{eff}}}{\mu z}, \text{ leading to } z^2 = \frac{2P_{c\text{eff}}K}{\mu} t, \quad (16)$$

where  $K$  is the medium's permeability and we have assumed  
 that at time  $t = 0$  no wetting fluid has yet invaded the medium.  
 If we choose to non-dimensionalize time by the character-  
 istic time  $(\mu L^2)/(P_{c\text{eff}}K)$ , we obtain from Eq. (16) the non-  
 dimensional equation  $Z^2 = 2T$ . Since, according to Bico  
 and Quéré's observation mentioned above, it is the lagging  
 (macroscopic) front that carries most of the interface between  
 the two fluids, Eq. 16, and therefore its non-dimensional coun-  
 terpart, can be assumed to describe the behavior of the lag-  
 ging front. From the experimental data for the lagging front,  
 $(P_{c\text{eff}}K)/(\mu L^2)$  is measured to be  $9.7 \cdot 10^{-5} \text{ s}^{-1}$ , which we  
 thus use to non-dimensionalize all plots in Fig. 13. The de-  
 pendence of  $Z^2$  on  $T$  for the lagging (macroscopic) front then  
 has a slope 2 (as shown by the dotted gray line in Fig. 13),  
 while that for the leading (microscopic) front exhibits a larger  
 imbibition rate, with a slope 2.67 (as shown by the orange  
 dotted line in Fig. 13).

#### IV. CONCLUSIONS

In conclusion, we investigated spontaneous imbibition of a  
 wetting fluid in a randomly arranged planar system of inter-  
 acting capillaries. This generalized model can predict the im-  
 bibition behavior for all the  $n!/2$  possible arrangements of an  
 interacting  $n$ -capillary system. It is inspired from a previous  
 work on stratified geological formations, with planar layers  
 instead of cylindrical capillaries.

Using an interacting capillary system containing 4 capillar-  
 ies, we showed that the imbibition dynamics depends signifi-  
 cantly on the arrangement of the capillaries within the capil-  
 lary system, for a given distribution of the capillary radii. Sim-  
 ilarly, the dynamics are affected by that distribution for a given  
 arrangement of the capillaries. Furthermore, we showed that  
 the arrangement and radii distribution of the capillaries jointly  
 control the relative menisci's locations, the breakthrough time,  
 and which capillary carries the leading meniscus. The cross-  
 sectional saturation of the impregnating fluid along the length  
 of the capillary system also changes with a change in the ar-  
 rangement of the capillaries. However, the total capillary pres-  
 sure driving the flow is identical for all arrangements, there-  
 fore, the overall volume fraction occupied by the invading  
 fluid (i.e., the global saturation of the wetting fluid) at a given  
 time remains the same across all arrangements, until break-  
 through occurs in one of the arrangements.

Similarly, considering 1000 randomly-chosen different ar-  
 rangements of an interacting twenty-capillary system having  
 uniform distribution of radii between 10 m and 200 m, we ob-  
 served that, depending on the arrangement of the capillaries,  
 the leading meniscus can be in any of the capillaries whose  
 radii are between 10 m and 100 m, and the non-dimensional  
 breakthrough time lies between  $T_{\text{bt}} = 0.31$  and  $T_{\text{bt}} = 0.42$ .

The dynamics of spontaneous imbibition as predicted by  
 this new model is significantly different from that predicted by  
 the classic bundle of non-interactive capillaries (or tubes), for  
 which the leading meniscus is always in the largest capil-  
 lary. For the interacting multi-capillary system mentioned  
 above, on the contrary, the leading meniscus can be in any  
 of the capillaries having radii between 10 m and 100 m. We  
 observed that the breakthrough occurs earlier than in the clas-  
 sic capillary bundle, where it occurs at non-dimensional time  
 $T_{\text{bt}} = 0.5$  for the aforementioned 20-capillary-system, to be  
 compared to the 0.31–0.42 range for the 20-capillary-system  
 mentioned above. Furthermore, for this system the saturation  
 at breakthrough time falls in the range 0.69–0.79, whereas for  
 the classic capillary bundle it is equal to 0.86. The dependence  
 of the saturation as a function of the longitudinal position are  
 also shows a stark contrast between the predictions of the clas-  
 sic capillary bundle and the average behavior of the 1000 ar-  
 rangements of interacting capillaries. Indeed, the interacting  
 capillary system shows a steep decrease in the saturation with  
 length as compared to the classic capillary bundle. Addition-  
 ally, the interacting multi-capillary system shows that the spa-  
 tial arrangement of the capillaries may cause significantly dif-  
 ferent saturation values at a given longitudinal position.

So, how is this model consisting of a planar bundle of inter-  
 acting capillaries to be used to predict spontaneous imbibition  
 in quasi-two-dimensional porous media whose pore size dis-  
 tribution is known? We propose to use a stochastic approach,  
 i.e., to consider the average behavior between a large number  
 of randomly-picked spatial arrangements of the capillary di-  
 ameters, the distribution of these diameters being equal to the  
 pore size distribution of the real porous medium. We tested  
 that method against data from the literature. Firstly, qualita-  
 tive observations relative to which ranges of pore sizes mainly  
 contribute to the leading and lagging fronts of the imbibition  
 interface, and to the longitudinal saturation profile, are consis-  
 tent between experiments from the literature and the predic-  
 tions of our model. Secondly, to validate the model's quanti-  
 tative predictive capacity, we compared its predictions to im-  
 bibition measurements in filter paper, performed by Bico and  
 Quéré<sup>47</sup>. The model predicts that the visible leading front is  
 carried by smaller pores and that the bulk saturating front re-  
 sponsible for most of the fluid mass invasion is the lagging  
 front carried by larger pores, which agrees very well with  
 the experimental findings. The quantitative predictions for  
 the positions in time of these two fronts, obtained from av-  
 eraging over the statistics of randomly-chosen arrangements,  
 agree well with the measurements.

This generalized model for spontaneous imbibition in a pla-  
 nar bundle of interacting capillaries, which is semi-analytical  
 and runs extremely quickly, could be useful for fast as-  
 sessment of one-dimensional imbibition dynamics in design-  
 based porous media such as loop heat pipes, diagnostic  
 devices and microfluidic devices, or in real porous media  
 whose porosity structure can reasonably be considered two-  
 dimensional, e.g., paper, thin porous media in general, or lay-  
 ered aquifers.

Prospects to this work include extending this approach to  
 three-dimensional models by considering parallel capillaries,

867 the positions of whose axes in a transverse plane would be the  
868 nodes of a triangular grid.

## 869 CONFLICTS OF INTEREST

870 There are no conflicts to declare.

## 871 ACKNOWLEDGEMENT

872 SA and YM acknowledge the financial support granted by  
873 the French Agence Nationale de la Recherche, under project  
874 CO2-3D with project number ANR-16-CE06-0001.

## 875 Appendix A: Mathematical formulation for the system of four 876 interacting capillaires

877 In capillary  $\alpha$ , for  $0 < z < z_\alpha(t)$ , the pressure drop is given  
878 by the Hagen-Poiseuille law as,

$$P(z_\alpha(t), t) - P_0 = -\frac{8\mu z_\alpha(t)}{r_\alpha^2} v_\alpha(t), \quad (\text{A1})$$

879 where  $\mu$  is the imbibing fluid's viscosity,  $v_\alpha(t)$  is the instan-  
880 taneous velocity of the wetting fluid in the capillary  $\alpha$ ,  $P_0$  is the  
881 inlet pressure and  $P(z_\alpha(t), t)$  is the pressure in the imbibing  
882 fluid at  $z_\alpha(t)$ , as shown in Fig. 3. Since the pressure fields are  
883 identical in all capillaries for  $z < z_\alpha(t)$ , the pressure gradient  
884 is the same in all capillaries, which from Eq. (A1) implies

$$\frac{v_\alpha(t)}{r_\alpha^2} = \frac{v_\beta(t)}{r_\beta^2} = \frac{v_\gamma(t)}{r_\gamma^2} = \frac{v_\delta(t)}{r_\delta^2}, \quad (\text{A2})$$

885 where the index  $i$  ( $i = \alpha, \beta, \gamma, \delta$ ) indicates quantities relative  
886 to the capillary of radius  $r_i$  and  $v_i(t)$  ( $i = \alpha, \beta, \gamma, \delta$ ) is the ve-  
887 locity of the imbibing fluid for  $z < z_\alpha(t)$ .

888 The capillary pressure jump through the fluid-fluid interface  
889 is  $P_{c\alpha}$  at  $z_\alpha(t)$ , where some of the imbibing fluid transfers  
890 from the capillary  $\alpha$  to other capillaries. The volumetric fluid  
891 transfer from the capillary  $\alpha$  to the capillaries  $\beta$  and  $\gamma$  is  $dq_\alpha$ ,  
892 whereas the fluid transfer from the capillary  $\alpha$  to the capillary  
893  $\delta$  is  $dq'_\alpha$ . The velocity of the advancing meniscus in capillary  
894  $\alpha$ ,  $dz_\alpha/dt$ , is thus given by

$$\frac{dz_\alpha}{dt} = v_\alpha(t) - \frac{dq_\alpha + dq'_\alpha}{\pi r_\alpha^2}. \quad (\text{A3})$$

895 For  $z_\alpha(t) < z < z_\delta(t)$ , the velocity of the fluid in capillary  $\delta$  is  
896 similarly given by

$$\frac{dz_\delta}{dt} = v_\delta(t) + \frac{dq'_\alpha}{\pi r_\delta^2}, \quad (\text{A4})$$

897 so the pressure drop in the capillary  $\delta$  between  $z = z_\alpha(t)$  and  
898  $z = z_\delta(t)$  is

$$P(z_\delta(t), t) - P(z_\alpha(t), t) = -\frac{8\mu(z_\delta(t) - z_\alpha(t))}{r_\delta^2} \left( v_\delta(t) + \frac{dq'_\alpha}{\pi r_\delta^2} \right). \quad (\text{A5})$$

At  $z = z_\delta(t)$ , the pressure jump across the meniscus is  $P_{c\delta}$ ,  
since the pressure in the non-wetting fluid is the atmospheric  
pressure.

The capillaries  $\beta$  and  $\gamma$  are on the other side of the capillary  
 $\alpha$  with respect to the capillary  $\delta$ . As the capillary pressure  
jump of the capillary  $\beta$  is smaller than that in the capillary  $\gamma$ ,  
the meniscus in  $\beta$  lags behind that in  $\gamma$ . Hence, the imbibing  
fluid in these capillaries is continuous for  $z_\alpha(t) < z < z_\beta(t)$ .  
Defining  $\omega$  and  $(1 - \omega)$  as the fractions of  $dq_\alpha$  transferred  
respectively to  $\beta$  and  $\gamma$ , we can write an equation similar to  
Eq. (A4) for both  $\beta$  and  $\alpha$ , where  $\omega dq_\alpha$  and  $(1 - \omega) dq_\alpha$  ap-  
pear respectively as a differential velocity term arising from  
fluid transfer. Considering that the pressure field is the same  
in the capillaries  $\beta$  and  $\gamma$  for  $z_\alpha(t) < z < z_\beta(t)$ , we then obtain  
in that  $z$  range:

$$\frac{v_\beta(t) + \frac{\omega dq_\alpha}{\pi r_\beta^2}}{\pi r_\beta^2} = \frac{v_\gamma(t) + \frac{(1-\omega) dq_\alpha}{\pi r_\gamma^2}}{\pi r_\gamma^2}. \quad (\text{A6})$$

Combining Eq. (A2) and Eq. (A6), we then obtain the fraction  
 $\omega$  from the capillaries' radii:  $\omega = r_\beta^4 / (r_\beta^4 + r_\gamma^4)$ . Therefore, the  
pressure drop in capillaries  $\beta$  and  $\gamma$  for  $z_\alpha(t) < z < z_\beta(t)$  is

$$P(z_\beta(t), t) - P(z_\alpha(t), t) = -\frac{8\mu(z_\beta(t) - z_\alpha(t))}{r_\beta^2} \left( v_\beta(t) + \omega \frac{dq_\alpha}{A_\beta} \right). \quad (\text{A7})$$

At the meniscus in the capillary  $\beta$ , the capillary pressure jump  
is  $P_{c\beta}$  and some of the impregnating fluid transfers from  $\beta$   
to  $\gamma$ , which we assume to correspond to a differential flow  
rate  $dq_\beta$ . The velocity of the meniscus in the capillary  $\beta$  for  
 $z > z_\beta(t)$  is then

$$\frac{dz_\beta}{dt} = v_\beta(t) + \omega \frac{dq_\alpha}{\pi r_\beta^2} - \frac{dq_\beta}{\pi r_\beta^2}. \quad (\text{A8})$$

Similarly, for  $z > z_\beta(t)$ , the meniscus in the capillary  $\gamma$  trav-  
els with a velocity given by

$$\frac{dz_\gamma}{dt} = v_\gamma(t) + (1 - \omega) \frac{dq_\alpha}{\pi r_\gamma^2} + \frac{dq_\beta}{\pi r_\gamma^2}. \quad (\text{A9})$$

The pressure drop between  $z = z_\beta(t)$  and  $z = z_\gamma(t)$  in capillary  
 $\gamma$  is then given by,

$$P(z_\gamma(t), t) - P(z_\beta(t), t) = -\frac{8\mu(z_\gamma(t) - z_\beta(t))}{r_\gamma^2} \left( v_\gamma(t) + (1 - \omega) \frac{dq_\alpha}{\pi r_\gamma^2} + \frac{dq_\beta}{\pi r_\gamma^2} \right). \quad (\text{A10})$$

The pressure jump across the meniscus in each of the  
capillaries is given by the Young-Laplace equation<sup>64,65</sup>, i.e.,  
Eq. (2), from which it follows that

$$P(z_i, t) - P_0 = -P_{c_i} = -\frac{2\sigma \cos \theta_w}{r_i}, \quad (\text{A11})$$

for  $i = \alpha, \beta, \gamma, \delta$ . Note that the prefactor 2 is controlled by circular cross-section of the tube, another geometry (e.g., square cross section) would yield a different prefactor. Eq. (A11) poses the total pressure drop within the impregnating wetting fluid in each of the capillaries. Substituting Eqs. (A3), (A4), (A8), (A9) in Eqs. (A1), (A5), (A7), (A10) respectively, we obtain the equations governing the flow in the interacting capillary system:

$$Pc_\alpha = \frac{8\mu z_\alpha(t)}{r_\alpha^4 + r_\beta^4 + r_\gamma^4 + r_\delta^4} \left( r_\alpha^2 \frac{dz_\alpha}{dt} + r_\beta^2 \frac{dz_\beta}{dt} + r_\gamma^2 \frac{dz_\gamma}{dt} + r_\delta^2 \frac{dz_\delta}{dt} \right) \quad (A12)$$

$$Pc_\delta - Pc_\alpha = \frac{8\mu(z_\delta(t) - z_\alpha(t))}{r_\delta^2} \left( \frac{dz_\delta}{dt} \right), \quad (A13)$$

$$Pc_\beta - Pc_\alpha = \frac{8\mu(z_\beta(t) - z_\alpha(t))}{r_\beta^4 + r_\gamma^4} \left( r_\beta^2 \frac{dz_\beta}{dt} + r_\gamma^2 \frac{dz_\gamma}{dt} \right), \quad (A14)$$

$$Pc_\gamma - Pc_\beta = \frac{8\mu(z_\gamma(t) - z_\beta(t))}{r_\gamma^2} \left( \frac{dz_\gamma}{dt} \right). \quad (A15)$$

## Appendix B: Generalization of the model for an arbitrary number of capillaires

The following step-by-step procedure must be followed:

1. We initiate the model formulation by finding the largest radius capillary,  $C_i$ . The pressure field is identical in all capillaries for  $z < z_a(t)$ , and the corresponding pressure gradient is related to the fluid velocity in each capillary, by Hagen-Poiseuille's law. Some of the invading fluid from capillary  $i$  transfers to other capillaries in the immediate vicinity of the meniscus position  $z_a(t)$ .
2. For  $z > z_a(t)$ , the imbibing fluid in the capillaries  $C_1$  to  $C_{(i-1)}$  is separated from the imbibing fluid in the capillaries  $C_{(i+1)}$  to  $C_n$ . We thus classify the capillaries on either sides of the capillary  $C_i$  in two regions, the capillaries  $C_1$  to  $C_{(i-1)}$  in the first one, the capillaries from  $C_{(i+1)}$  to  $C_n$  in another one. The fluid transfer from the capillary  $C_i$  is divided among the other capillaries according to their radii. If the fluid transfer to the 'top region' is  $dq_t$ , the fraction of  $dq_t$  flowing from capillary  $C_i$  to a capillary of radius  $r_p$  would be  $r_p^4 dq_t / \sum_{q=1}^{i-1} (r_q^4)$ . Similarly, for the 'bottom region', if  $dq_b$  is the fluid transfer from  $C_i$ , the fractional flow in a capillary of radius  $r_r$  will be  $r_r^4 dq_b / \sum_{s=i+1}^n (r_s^4)$ . This fluid transfer causes the flow rates to increase in capillaries  $C_1$  to  $C_{(i-1)}$  and  $C_{(i+1)}$  to  $C_n$ .
3. The widest capillary among the capillaries  $C_1$  to  $C_{(i-1)}$   $C_j$  is now identified. For  $z_a(t) < z < z_b(t)$  the pressure field in the imbibing fluid is identical in capillaries  $C_1$  to  $C_{(i-1)}$ , and is related to the fluid velocity in each capillary by Hagen-Poiseuille's law. In the vicinity of

$z = z_b(t)$ , some of the invading fluid transfers from  $C_j$  to the capillaries  $C_1$  to  $C_{(j-1)}$  and  $C_{(j+1)}$  to  $C_{(i-1)}$ , which increases the flow rate in these capillaries.

4. Similarly, the widest capillary among capillary  $C_{(i+1)}$  to  $C_n$ , which we denote  $C_k$ , is chosen. The pressure field is identical in the capillaries  $C_{(i+1)}$  to  $C_n$  for  $z_a(t) < z < z_c(t)$ , and the pressure gradient is related to the fluid velocity in each of these capillaries from the Hagen-Poiseuille law. At  $z = z_c(t)$ , some of the fluid invading  $C_k$  transfers into the capillaries  $C_{(i+1)}$  to  $C_{(k-1)}$  and  $C_{(k+1)}$  to  $C_n$ , which increases the flow rate in these capillaries.
5. The impregnating fluids in the regions encompassing capillaries  $C_1$  to  $C_{(j-1)}$  and  $C_{(j+1)}$  to  $C_{(i-1)}$  are separated by displaced fluid in capillary  $C_j$  for  $z > z_j$ . Again, the capillary of largest radius among the capillaries  $C_1$  to  $C_{(j-1)}$  is identified, as well as the capillary of largest radius among the capillaries  $C_{(j+1)}$  to  $C_{(i-1)}$ . The similar procedure previously explained for the pressure field and its relation to the fluid velocity is repeated for those two regions.
6. The same procedure as explained in step 5. is performed in the regions encompassing capillaries  $C_{(i+1)}$  to  $C_{(k-1)}$  and  $C_{(k+1)}$  to  $C_n$ .
7. This is repeated in all the regions which have been defined in steps 1 to 5, and this in a recursive manner, until the entire bundle of interacting capillaries is divided into regions containing only one capillary each.
8. The pressure jump across the meniscus in each of the capillaries is the corresponding Young-Laplace capillary pressure of that capillary. The  $n$  equations relating the pressure drops to the velocities of the fluid-fluid interfaces are then solved to obtain the lengths impregnated in each of the capillaries at the considered time  $t$ .

## Appendix C: Imbibition in all possible arrangements of a system of four interacting capillaries

A four capillary system has 12 possible arrangements. For a set of capillaries with radii  $r_\alpha = 80$  m,  $r_\beta = 60$  m,  $r_\gamma = 40$  m and  $r_\delta = 20$  m, we present in Fig. C.1 the time evolution of the menisci's positions in all four capillaries for all 12 arrangements.

We see from Fig. C.1 that the leading meniscus is in capillary  $\delta$  for arrangements shown in Fig. C.1(a),(b),(f),(g),(i),(j),(k),(l). For the arrangements shown in Fig. C.1(c),(d), the leading meniscus is in  $\gamma$ . For arrangements shown in Fig. C.1(e),(h), the capillaries  $\gamma$  and  $\delta$  impregnate the same distance with time. But the breakthrough times are different for all the arrangements, varying from  $T = 0.33$  to  $T = 0.40$ . The minimal breakthrough time is 0.33, observed in arrangements (a), (g), (k) and (l) of Fig. C.1.

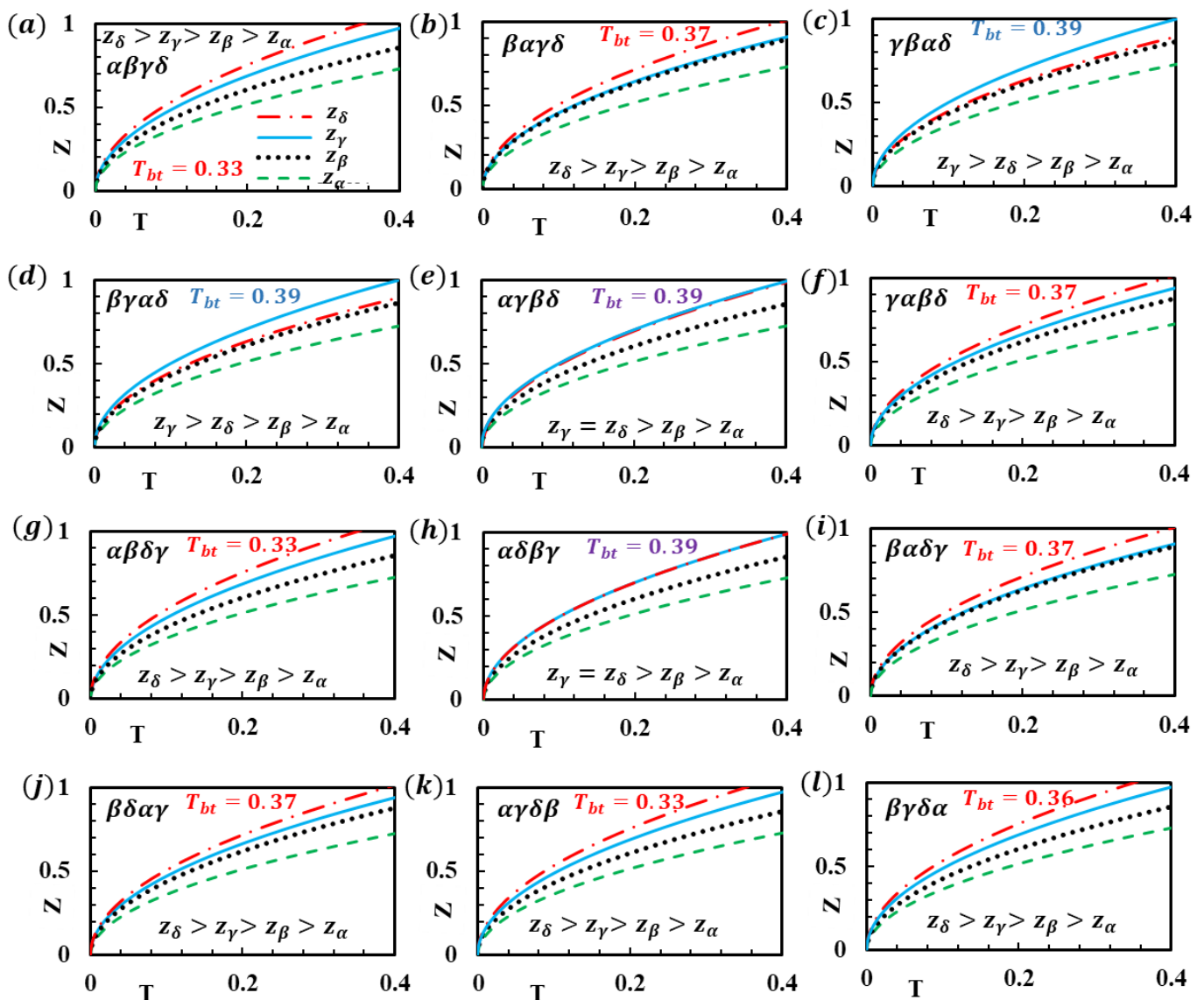


FIG. C.1. Spontaneous imbibition in a system of four interacting capillaries of radii  $r_\alpha = 80$  m,  $r_\beta = 60$  m,  $r_\gamma = 40$  m and  $r_\delta = 20$  m. The non-dimensional positions of the four menisci are shown as a function of non-dimensional time for all the 12 possible arrangements in (a) to (l). The arrangement, the ordering of the menisci locations, and the breakthrough times for each of the cases (a) to (l) are provided as legends of the plots.

1020 The breakthrough for all the arrangements shown in Fig. C.1  
1021 occurs between 225.7 s and 273.6 s.

#### 1022 Appendix D: Convergence of the computations for a system 1023 of 20 interacting capillaries

1024 For the study of the bundle consisting of 20 interacting cap-  
1025 illaries, the convergence of the results as a function of the  
1026 number of randomly-chosen spatial arrangements was verified  
1027 in the following manner.

1028 Three sets of  $R = 100$ , 1000 and 2000 randomly-chosen  
1029 arrangements were simulated independently, and their results  
1030 were compared with each other. Fig. D.1(a) shows the spa-

1031 tial profile of wetting phase saturation at three different times  
1032 ( $T = 0.2$ ,  $T = 0.3$ ,  $T = T_{bt}$ ), obtained as the average of the  
1033 spatial profiles for all  $R$  arrangements. Fig. D.1(b) shows  
1034 the standard deviation over the statistics of the spatial wetting  
1035 phase saturation profiles for the  $R$  arrangement, also at times  
1036  $T = 0.2$ ,  $T = 0.3$ ,  $T = T_{bt}$ . Obviously the average behavior for  
1037 1000 arrangements (in contrast to the case  $R = 100$ ) cannot  
1038 be distinguished from that for 2000 arrangements, and even  
1039 the spatial profiles of the standard deviation over the statis-  
1040 tics are quite similar for the two cases. Therefore, we con-  
1041 sider  $R = 1000$  to be a sufficiently large number of randomly-  
1042 chosen arrangements for the imbibition dynamics to be well  
1043 predicted in a system of 20 interacting capillaries.

1044 <sup>1</sup>B. Xiao, J. Fan, and F. Ding, "Prediction of relative permeability of unsat-

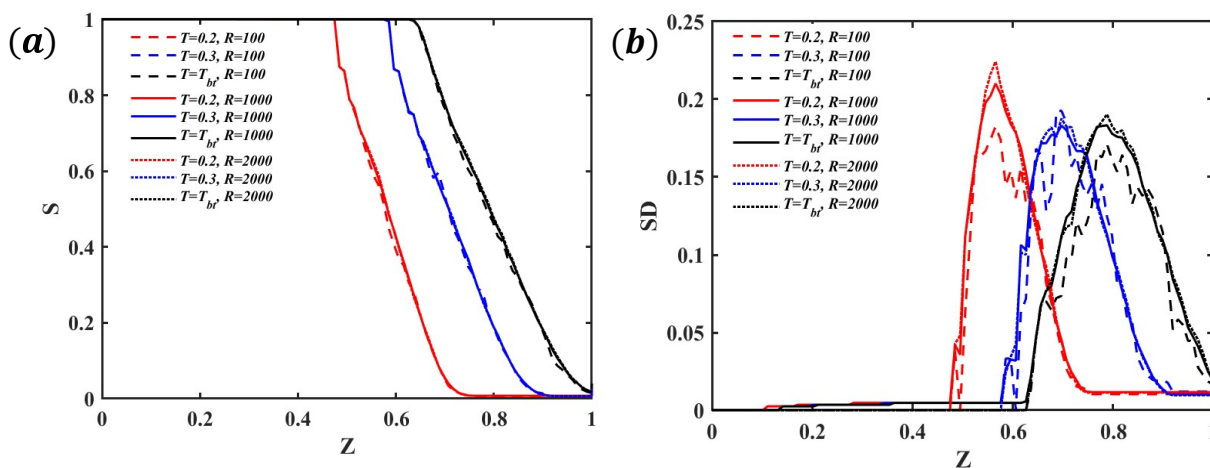
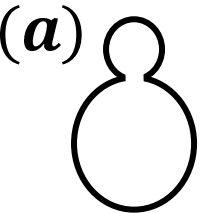


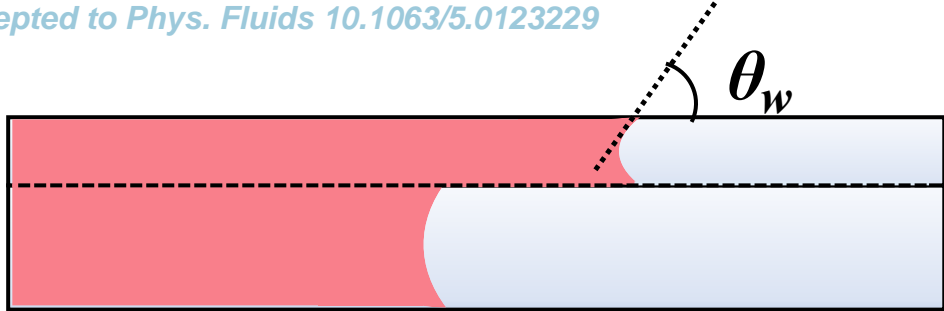
FIG. D.1. Convergence of the simulations for a system of 20 interacting capillaries, based on  $R = 100, 1000$  and  $2000$  arrangements at  $T = 0.2, T = 0.3$ , and  $T = T_{bt}$  (breakthrough time): (a) Mean saturation as a function of the longitudinal coordinate. (b) Standard deviation (SD) of the statistics as a function of the longitudinal coordinate.

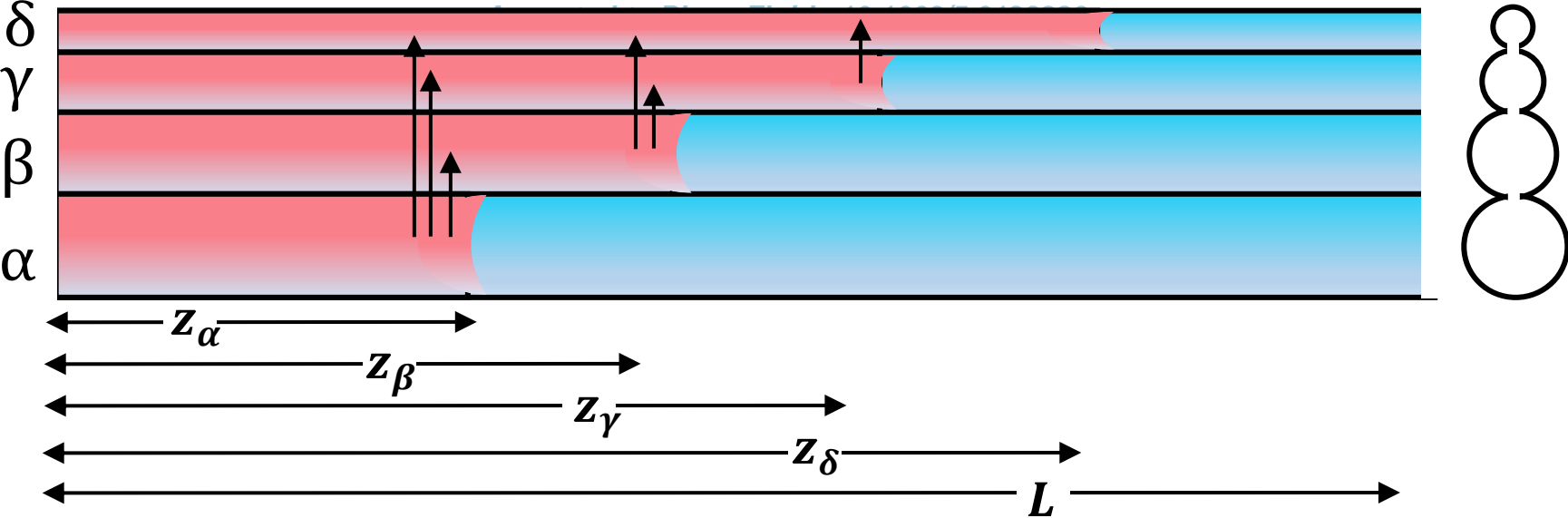
- 1046 urated porous media based on fractal theory and monte carlo simulation, *Energy & fuels* **26**, 6971–6978 (2012). 1092
- 1047 2Y.-J. Lin, P. He, M. Tavakkoli, N. T. Mathew, Y. Y. Fatt, J. C. Chai, A. G. 1093
- 1048 harzadeh, F. M. Vargas, and S. L. Biswal, “Characterizing asphaltene depo- 1094
- 1049 sition in the presence of chemical dispersants in porous media micromod- 1095
- 1050 els,” *Energy & fuels* **31**, 11660–11668 (2017). 1096
- 1051 3S. Saraji, L. Goual, and M. Piri, “Adsorption of asphaltenes in porous 1097
- 1052 media under flow conditions,” *Energy & fuels* **24**, 6009–6017 (2010). 1098
- 1053 4M. Taghizadeh-Behbahani, B. Hemmateenejad, M. Shamsipur, and 1099
- 1054 A. Tavassoli, “A paper-based length of stain analytical device for naked eye 100
- 1055 (readout-free) detection of cystic fibrosis,” *Analytica Chimica Acta* (2019) 101
- 1056 5Y. Soda, D. Citterio, and E. Bakker, “Equipment-free detection of k+ on mi- 102
- 1057 crofluidic paper-based analytical devices based on exhaustive replacement 103
- 1058 with ionic dye in ion-selective capillary sensors,” *ACS sensors* **4**, 670–677 104
- 1059 (2019). 1105
- 1060 6B. Dai, K. Li, L. Shi, X. Wan, X. Liu, F. Zhang, L. Jiang, and S. Wang 106
- 1061 “Bioinspired janus textile with conical micropores for human body mois- 107
- 1062 ture and thermal management,” *Advanced Materials* (2019). 1108
- 1063 7M. Rosello, S. Sur, B. Barbet, and J. P. Rothstein, “Dripping-onto-substrate 109
- 1064 capillary breakup extensional rheometry of low-viscosity printing inks 110
- 1065 Journal of Non-Newtonian Fluid Mechanics **266**, 160–170 (2019). 1111
- 1066 8Y. Wang, R. Deng, L. Yang, and C. D. Bain, “Fabrication of monolayers of 112
- 1067 uniform polymeric particles by inkjet printing of monodisperse emulsions 113
- 1068 produced by microfluidics,” *Lab on a Chip* **19**, 3077–3085 (2019). 1114
- 1069 9Y. Liu, J. Kaszuba, and J. Oakey, “Microfluidic investigations of crude oil 115
- 1070 brine interface elasticity modifications via brine chemistry to enhance oil 116
- 1071 recovery,” *Fuel* **239**, 338–346 (2019). 1117
- 1072 10R. Gharibshahi, M. Omidkhan, A. Jafari, and Z. Fakhroueian, “Hybridiza- 118
- 1073 tion of superparamagnetic fe3o4 nanoparticles with mwcnts and effect of 119
- 1074 surface modification on electromagnetic heating process efficiency: A mi- 120
- 1075 crofluidics enhanced oil recovery study,” *Fuel* **282**, 118603 (2020). 1121
- 1076 11C. Carrell, A. Kava, M. Nguyen, R. Menger, Z. Munshi, Z. Call, M. Nuss- 122
- 1077 baum, and C. Henry, “Beyond the lateral flow assay: A review of paper- 123
- 1078 based microfluidics,” *Microelectronic Engineering* **206**, 45–54 (2019). 1124
- 1079 12F. Schaumburg and C. L. Berli, “Assessing the rapid flow in multilay- 125
- 1080 er paper-based microfluidic devices,” *Microfluidics and Nanofluidics* **23**, 98 126
- 1081 (2019). 1127
- 1082 13M. Rich, O. Mohd, F. S. Ligler, and G. M. Walker, “Characterization 128
- 1083 of glass frit capillary pumps for microfluidic devices,” *Microfluidics and 129*
- 1084 *Nanofluidics* **23**, 70 (2019). 1130
- 1085 14J.-H. Lin, W.-H. Chen, Y.-J. Su, and T.-H. Ko, “Performance analysis of 131
- 1086 a proton-exchange membrane fuel cell (pemfc) with various hydrophobic 132
- 1087 agents in a gas diffusion layer,” *Energy & fuels* **22**, 1200–1203 (2008). 1133
- 1088 15K. K. Lee, M.-O. Kim, and S. Choi, “A whole blood sample-to-answer 134
- 1089 polymer lab-on-a-chip with superhydrophilic surface toward point-of-care 135
- 1090 technology,” *Journal of pharmaceutical and biomedical analysis* **162**, 28–33 (2019).
- 1091 16C. Liang, Y. Liu, A. Niu, C. Liu, J. Li, and D. Ning, “Smartphone-app 136
- 1092 based point-of-care testing for myocardial infarction biomarker ctnt using 137
- 1093 an autonomous capillary microfluidic chip with self-aligned on-chip focus- 138
- 1094 ing (sof) lenses,” *Lab on a Chip* **19**, 1797–1807 (2019).
- 1095 17H.-A. Joung, Z. S. Ballard, A. Ma, D. K. Tseng, H. Teshome, S. Bu- 139
- 1096 rakowski, O. B. Garner, D. Di Carlo, and A. Ozcan, “based multiplexed 140
- 1097 vertical flow assay for point-of-care testing,” *Lab on a Chip* **19**, 1027–1034 (2019).
- 1098 18B. Xiao, W. Wang, X. Zhang, G. Long, H. Chen, H. Cai, and L. Deng, “A 141
- 1099 novel fractal model for relative permeability of gas diffusion layer in proton 142
- 1100 exchange membrane fuel cell with capillary pressure effect,” *Fractals* **27**, 1950012 (2019).
- 1101 19P. Carrere and M. Prat, “Liquid water in cathode gas diffusion layers of pem 143
- 1102 fuel cells: Identification of various pore filling regimes from pore network 144
- 1103 simulations,” *International Journal of Heat and Mass Transfer* **129**, 1043– 145
- 1104 1056 (2019).
- 1105 20M. Singh, N. V. Datla, S. Kondaraju, and S. S. Bahga, “Enhanced thermal 146
- 1106 performance of micro heat pipes through optimization of wettability 147
- 1107 gradient,” *Applied Thermal Engineering* **143**, 350–357 (2018).
- 1108 21M. Chernysheva and Y. Maydanik, “Simulation of heat and mass transfer in 148
- 1109 a cylindrical evaporator of a loop heat pipe,” *International Journal of Heat 149*
- 1110 and Mass Transfer **131**, 442–449 (2019).
- 1111 22C. Pozrikidis, “Axisymmetric motion of a file of red blood cells through 150
- 1112 capillaries,” *Physics of fluids* **17**, 031503 (2005).
- 1113 23K. Singh, B. P. Muljadi, A. Q. Raelini, C. Jost, V. Vandeginste, M. J. Blunt, 151
- 1114 G. Theraulaz, and P. Degond, “The architectural design of smart ventila- 152
- 1115 tion and drainage systems in termite nests,” *Science advances* **5**, eaat8520 153
- 1116 (2019).
- 1117 24K. Li, D. Zhang, H. Bian, C. Meng, and Y. Yang, “Criteria for applying the 154
- 1118 lucas-washburn law,” *Scientific reports* **5**, 14085 (2015).
- 1119 25S. Gruener and P. Huber, “Capillarity-driven oil flow in nanopores: Darcy 155
- 1120 scale analysis of lucas-washburn imbibition dynamics,” *Transport in Porous 156*
- 1121 Media **126**, 599–614 (2019).
- 1122 26J. Cai, Y. Chen, Y. Liu, S. Li, and C. Sun, “Capillary imbibition and flow 157
- 1123 of wetting liquid in irregular capillaries: A 100-year review,” *Advances in 158*
- 1124 Colloid and Interface Science , 102654 (2022).
- 1125 27R. Lucas, “Ueber das zeitgesetz des kapillaren aufstiegs von flüssigkeiten,” 159
- 1126 *Colloid & Polymer Science* **23**, 15–22 (1918).
- 1127 28E. Washburn, “The dynamics of capillary flow,” *Physical Review* **17**, 273 160
- 1128 (1921).
- 1129 29R. Lenormand, C. Zaccaro, *et al.*, “Role of roughness and edges during 161
- 1130 imbibition in square capillaries,” in *SPE annual technical conference and 162*
- 1131 *exhibition* (Society of Petroleum Engineers, 1984).

- 1136 <sup>30</sup>M. Dong and I. Chatzis, "The imbibition and flow of a wetting liquid along the  
1137 corners of a square capillary tube," *Journal of colloid and interface science* **199**  
1138 **172**, 278–288 (1995). 1200
- 1139 <sup>31</sup>M. Ramezanzadeh, S. Khasi, and M. H. Ghazanfari, "Simulating imbibition  
1140 process using interacting capillary bundle model with corner flow: The role  
1141 of capillary morphology," *Journal of Petroleum Science and Engineering* **176**,  
1142 62–73 (2019). 1204
- 1143 <sup>32</sup>D. Zheng, W. Wang, and Z. Reza, "Integrated pore-scale characterization of  
1144 mercury injection/imbibition and isothermal adsorption/desorption experiments  
1145 using dendroidal model for shales," *Journal of Petroleum Science and Engineering*  
1146 **178**, 751–765 (2019). 1208
- 1147 <sup>33</sup>M. Reyssat, L. Courbin, E. Reyssat, and H. A. Stone, "Imbibition in geometries  
1148 with axial variations," *Journal of Fluid Mechanics* **615**, 335–344 (2008).  
1149 1211
- 1150 <sup>34</sup>A. Budaraju, J. Phirani, S. Kondaraju, and S. S. Bahga, "Capillary displacement of  
1151 viscous liquids in geometries with axial variations," *Langmuir* **32**, 10513–10521  
1152 (2016). 1212
- 1153 <sup>35</sup>F. F. Ouali, G. McHale, H. Javed, C. Trabi, N. J. Shirtcliffe, and M. I. Newton,  
1154 "Wetting considerations in capillary rise and imbibition in closed square  
1155 tubes and open rectangular cross-section channels," *Microfluidics and nanofluidics*  
1156 **15**, 309–326 (2013). 1215
- 1157 <sup>36</sup>U. Rosendahl, A. Grah, and M. E. Dreyer, "Convective dominated flows in open  
1158 capillary channels," *Physics of Fluids* **22**, 052102 (2010). 1218
- 1159 <sup>37</sup>M. M. Weislogel, "Capillary flow in interior corners: The infinite column,"  
1160 *Physics of Fluids* **13**, 3101–3107 (2001). 1219
- 1161 <sup>38</sup>D. Dimitrov, L. Klushin, A. Milchev, and K. Binder, "Flow and transport in  
1162 brush-coated capillaries: A molecular dynamics simulation," *Physics of Fluids*  
1163 **20**, 092102 (2008). 1222
- 1164 <sup>39</sup>J. Wang, A. Salama, and J. Kou, "Experimental and numerical analysis of  
1165 imbibition processes in a corrugated capillary tube," *Capillarity* **5**, 83–90  
1166 (2022). 1225
- 1167 <sup>40</sup>A. Salama, "On the dynamics of a meniscus inside capillaries during imbibition  
1168 and drainage processes: A generalized model, effect of inertia, and numerical  
1169 algorithm," *Physics of Fluids* **33**, 082104 (2021). 1228
- 1170 <sup>41</sup>H. K. Dahle, M. A. Celia, and S. M. Hassanzadeh, "Bundle-of-tubes model for  
1171 calculating dynamic effects in the capillary-pressure-saturation relationship,"  
1172 *Transport in Porous media* **58**, 5–22 (2005). 1230
- 1173 <sup>42</sup>R. Douglas and J. Bartley, "Capillary tube models with interaction between the  
1174 tubes [a note on "immiscible displacement in the interacting capillary bundle  
1175 model part i. development of interacting capillary bundle model" by dong, m.,  
1176 dullien, fal, dai, l. and li, d., 2005, transport porous media]," *Transport in  
1177 porous media* **86**, 479–482 (2011). 1232
- 1178 <sup>43</sup>J. Bartley and D. Ruth, "Relative permeability analysis of tube bundle models,  
1179 including capillary pressure," *Transport in porous media* **45**, 445–478 (2001).  
1180 1233
- 1181 <sup>44</sup>J. Bartley and D. Ruth, "Relative permeability analysis of tube bundle models,"  
1182 *Transport in Porous Media* **36**, 161–188 (1999). 1234
- 1183 <sup>45</sup>Y. Shiri and S. M. J. Seyed Sabour, "Analytical, experimental, and numerical  
1184 study of capillary rise dynamics from inertial to viscous flow," *Physics of  
1185 Fluids* **34**, 102105 (2022). 1235
- 1186 <sup>46</sup>J. Kim, M.-W. Moon, and H.-Y. Kim, "Capillary rise in superhydrophilic  
1187 rough channels," *Physics of Fluids* **32**, 032105 (2020). 1236
- 1188 <sup>47</sup>J. Bico and D. Quéré, "Precursors of impregnation," *EPL (Europhysics Letters)*  
1189 **61**, 348 (2003). 1237
- 1190 <sup>48</sup>M. Dong, J. Zhou, *et al.*, "Characterization of waterflood saturation profiles  
1191 histories by the 'complete' capillary number," *Transport in porous media* **31**,  
1192 213–237 (1998). 1238
- 1193 <sup>49</sup>M. Dong, F. A. Dullien, L. Dai, and D. Li, "Immiscible displacement in the  
1194 interacting capillary bundle model part i. development of interacting  
1195 capillary bundle model," *Transport in Porous media* **59**, 1–18 (2005). 1239
- 1196 <sup>50</sup>M. Dong, F. A. Dullien, L. Dai, and D. Li, "Immiscible displacement in the  
1197 interacting capillary bundle model part ii. applications of model and comparison  
1198 of interacting and non-interacting capillary bundle models," *Transport in  
1199 Porous media* **63**, 289–304 (2006). 1240
- 1201 <sup>51</sup>S. Krishnamurthy and Y. Peles, "Gas-liquid two-phase flow across a bank  
1202 of micropillars," *Physics of fluids* **19**, 043302 (2007). 1241
- 1203 <sup>52</sup>J. Wang, F. A. Dullien, and M. Dong, "Fluid transfer between tubes in  
1204 interacting capillary bundle models," *Transport in Porous Media* **71**, 115–  
1205 131 (2008). 1242
- 1206 <sup>53</sup>S. Li, M. Dong, and P. Luo, "A crossflow model for an interacting capillary  
1207 bundle: Development and application for waterflooding in tight oil  
1208 reservoirs," *Chemical Engineering Science* **164**, 133–147 (2017). 1243
- 1209 <sup>54</sup>S. Ashraf, G. Visavale, S. S. Bahga, and J. Phirani, "Spontaneous imbibition  
1210 in parallel layers of packed beads," *The European Physical Journal E* **40**, 39  
1211 (2017). 1244
- 1212 <sup>55</sup>S. Ashraf, G. Visavale, and J. Phirani, "Spontaneous imbibition in randomly  
1213 arranged interacting capillaries," *Chemical Engineering Science* **192**, 218–234  
1214 (2018). 1245
- 1215 <sup>56</sup>E. Unsal, G. Mason, N. Morrow, and D. Ruth, "Co-current and counter-current  
1216 imbibition in independent tubes of non-axisymmetric geometry," *Journal of  
1217 Colloid and Interface Science* **306**, 105–117 (2007). 1246
- 1218 <sup>57</sup>E. Unsal, G. Mason, D. Ruth, and N. Morrow, "Co-and counter-current  
1219 spontaneous imbibition into groups of capillary tubes with lateral connections  
1220 permitting cross-flow," *Journal of Colloid and Interface Science* **315**,  
1221 200–209 (2007). 1247
- 1222 <sup>58</sup>E. Unsal, G. Mason, N. R. Morrow, and D. W. Ruth, "Bubble snap-off and  
1223 capillary-back pressure during counter-current spontaneous imbibition into  
1224 model pores," *Langmuir* **25**, 3387–3395 (2009). 1248
- 1225 <sup>59</sup>T. Bultreys, K. Singh, A. Q. Raeini, L. C. Ruspini, P.-E. Øren, S. Berg,  
1226 M. Rücker, B. Bijeljic, and M. J. Blunt, "Verifying pore network models of  
1227 imbibition in rocks using time-resolved synchrotron imaging," *Water  
1228 Resources Research* **56**, e2019WR026587 (2020). 1249
- 1229 <sup>60</sup>T. Bultreys, K. Singh, A. Q. Raeini, P.-E. Oren, S. Berg, B. Bijeljic, and  
1230 M. J. Blunt, "Improving the description of two-phase flow in rocks by  
1231 integrating pore scale models and experiments," in *InterPore 11th Annual  
1232 Meeting and Jubilee* (2019) p. 87. 1250
- 1233 <sup>61</sup>S. Foroughi, B. Bijeljic, and M. J. Blunt, "Pore-by-pore modelling, validation  
1234 and prediction of waterflooding in oil-wet rocks using dynamic synchrotron  
1235 data," *Transport in Porous Media* **138**, 285–308 (2021). 1251
- 1236 <sup>62</sup>S. Ashraf and J. Phirani, "A generalized model for spontaneous imbibition  
1237 in a horizontal, multi-layered porous medium," *Chemical Engineering Science*  
1238 **209**, 115175 (2019). 1252
- 1239 <sup>63</sup>C. W. Hirt and B. D. Nichols, "Volume of fluid (vof) method for the  
1240 dynamics of free boundaries," *Journal of computational physics* **39**, 201–225  
1241 (1981). 1253
- 1242 <sup>64</sup>T. Young, "III. an essay on the cohesion of fluids," *Philosophical Transactions  
1243 of the Royal Society of London* **95**, 65–87 (1805). 1254
- 1244 <sup>65</sup>P. S. de Laplace, *Supplément au dixième livre du Traité de mécanique  
1245 céleste: sur l'action capillaire* (1806). 1255
- 1246 <sup>66</sup>L. Ding, Q. Wu, L. Zhang, and D. Guérrillot, "Application of fractional flow  
1247 theory for analytical modeling of surfactant flooding, polymer flooding, and  
1248 surfactant/polymer flooding for chemical enhanced oil recovery," *Water* **12**,  
1249 2195 (2020). 1256
- 1250 <sup>67</sup>Y. Debbabi, M. D. Jackson, G. J. Hampson, P. J. Fitch, and P. Salinas,  
1251 "Viscous crossflow in layered porous media," *Transport in Porous Media*  
1252 **117**, 281–309 (2017). 1257
- 1253 <sup>68</sup>S. Akbari, S. M. Mahmood, H. Ghaedi, and S. Al-Hajri, "A new empirical  
1254 model for viscosity of sulfonated polyacrylamide polymers," *Polymers* **11**,  
1255 1046 (2019). 1258
- 1256 <sup>69</sup>S. Ashraf and J. Phirani, "Capillary displacement of viscous liquids in a  
1257 multi-layered porous medium," *Soft matter* **15**, 2057–2070 (2019). 1259
- 1258 <sup>70</sup>S. Ashraf and J. Phirani, "Capillary impregnation of viscous fluids in a  
1259 multi-layered porous medium," in *Fluids Engineering Division Summer  
1260 Meeting*, Vol. 59087 (American Society of Mechanical Engineers, 2019)  
p. V005T05A057. 1260

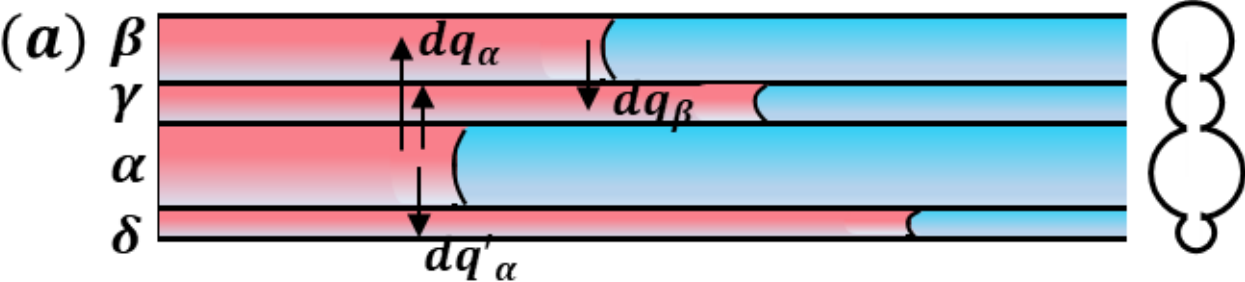


(b)

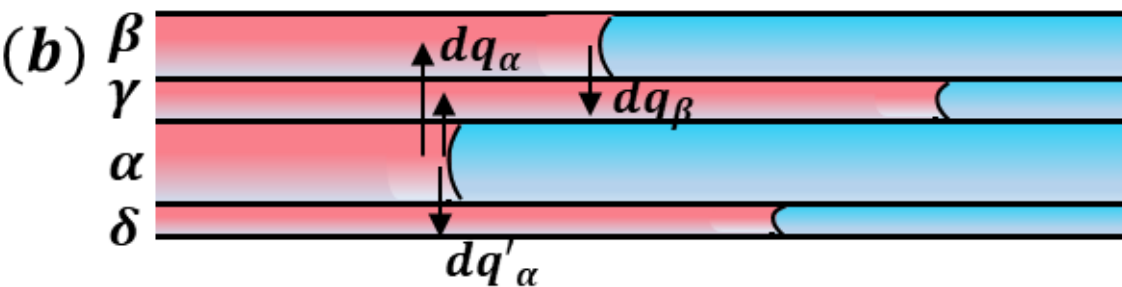




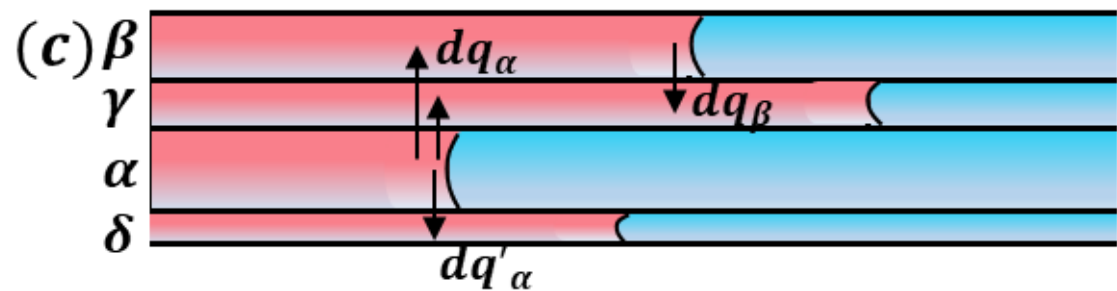
$$z_\delta > z_\gamma > z_\beta > z_\alpha$$

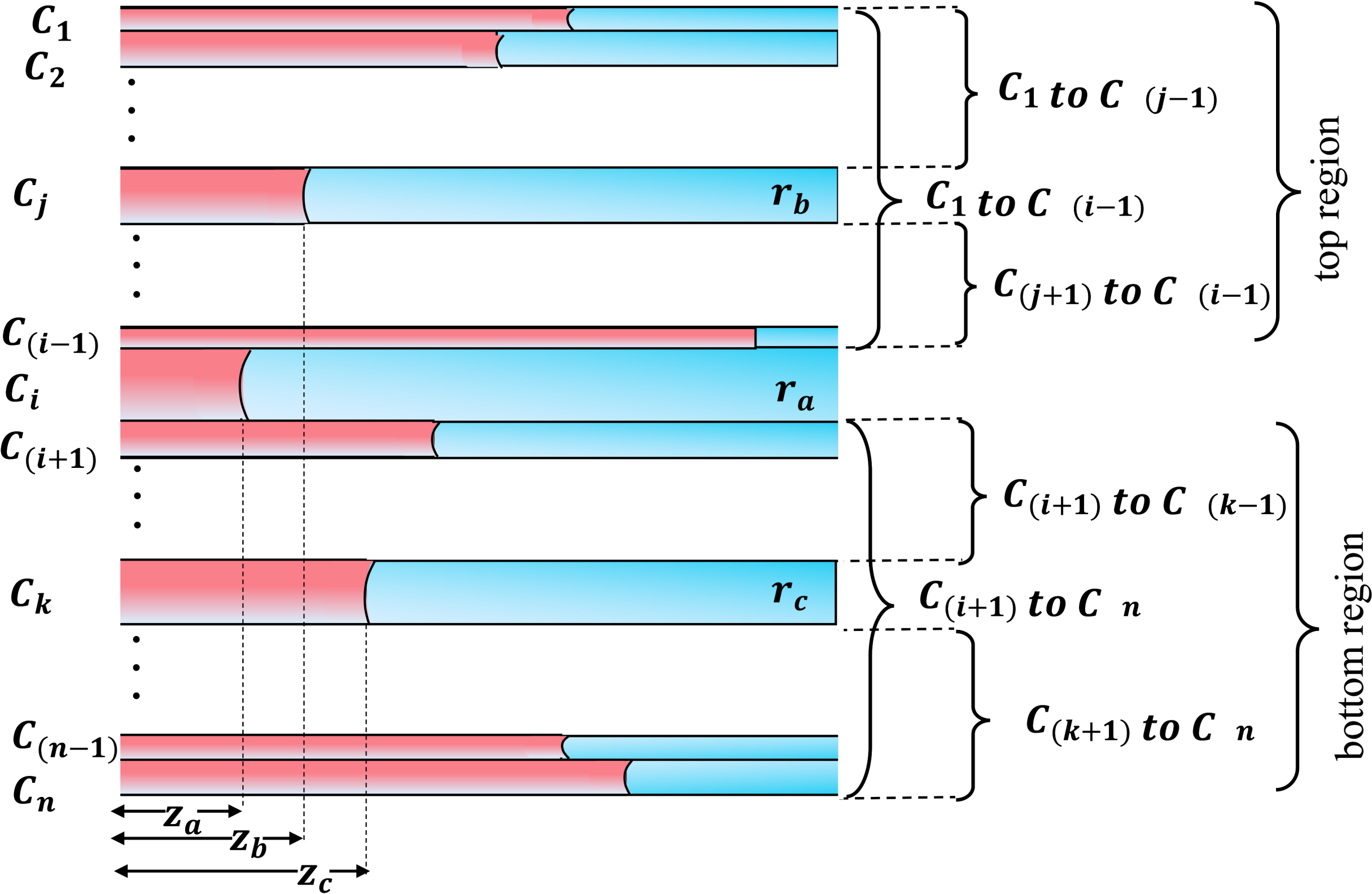


$$z_\gamma > z_\delta > z_\beta > z_\alpha$$

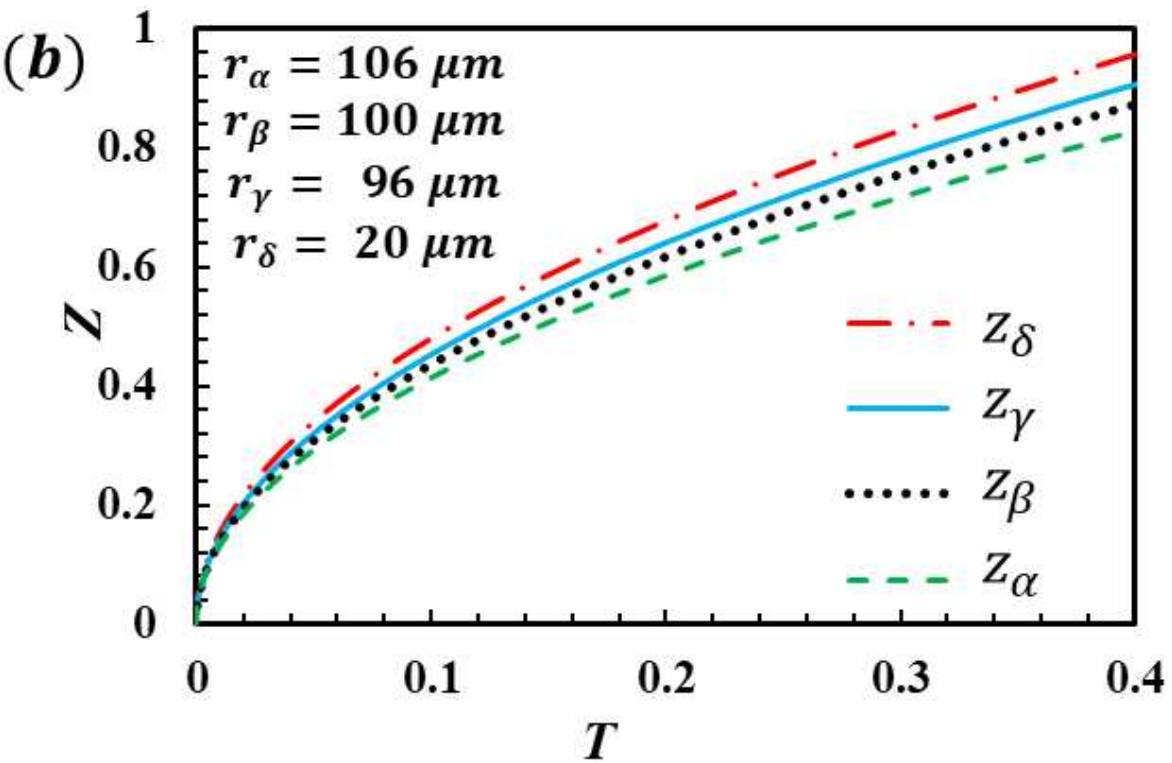
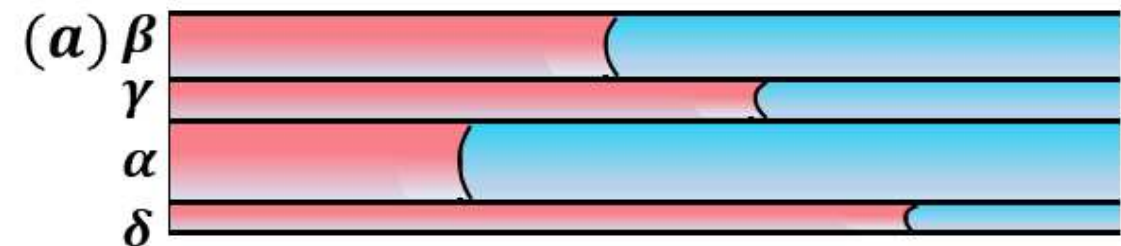


$$z_\gamma > z_\beta > z_\delta > z_\alpha$$

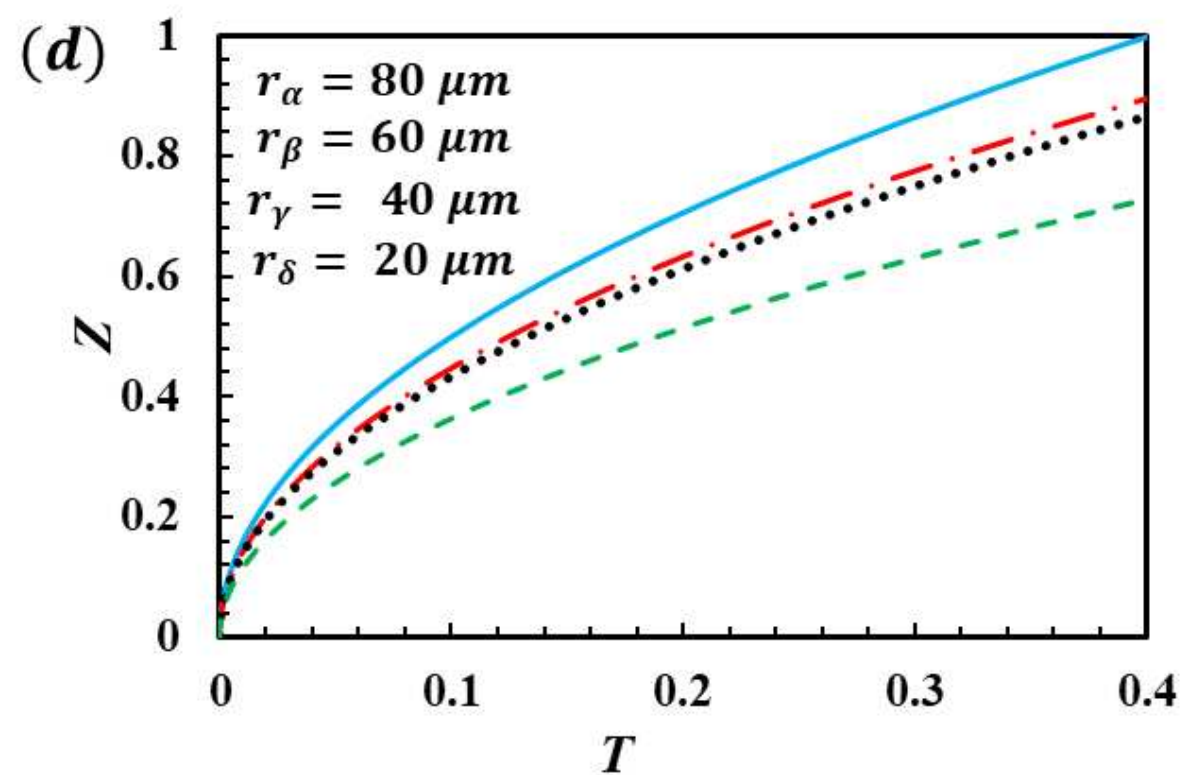
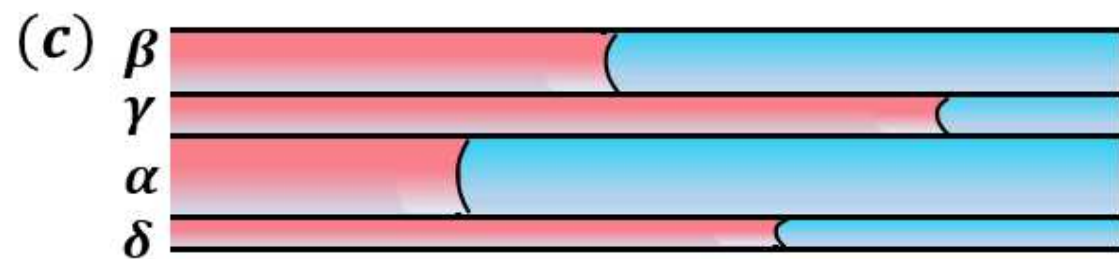




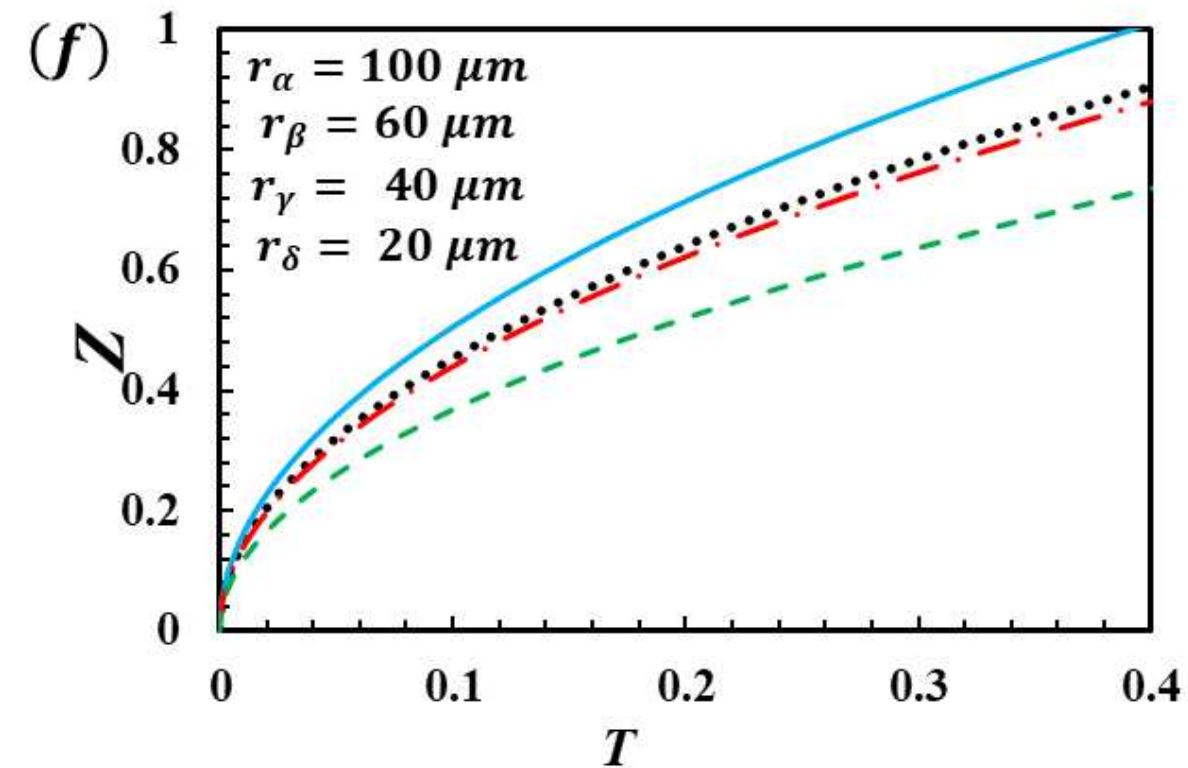
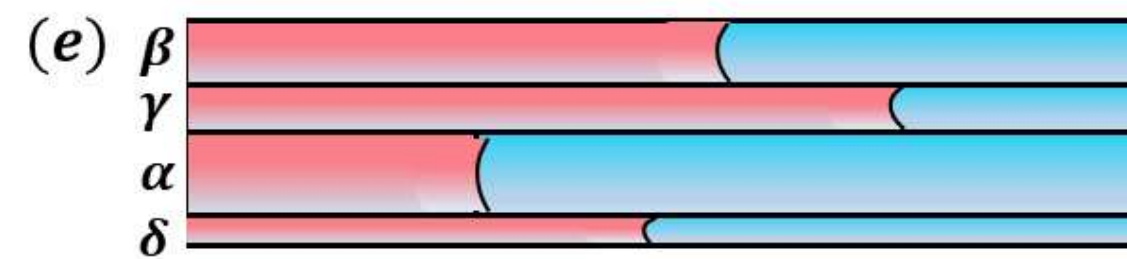
$$z_\delta > z_\gamma > z_\beta > z_\alpha$$



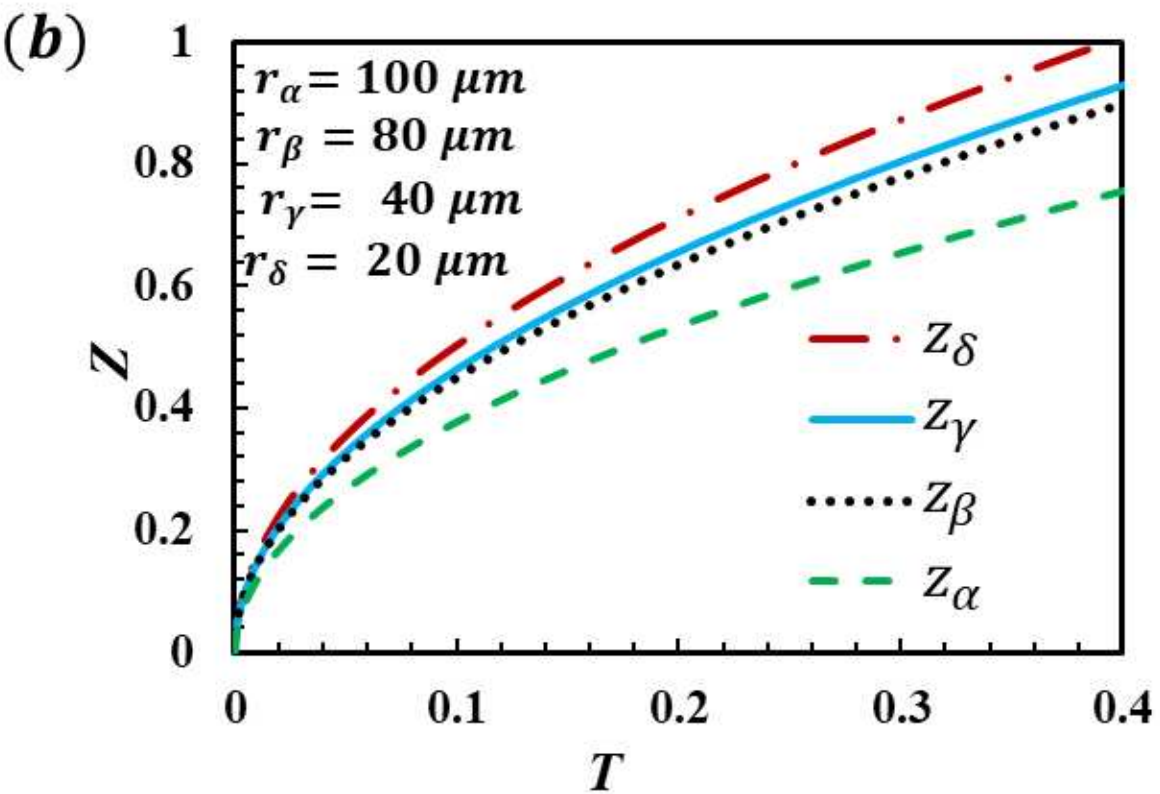
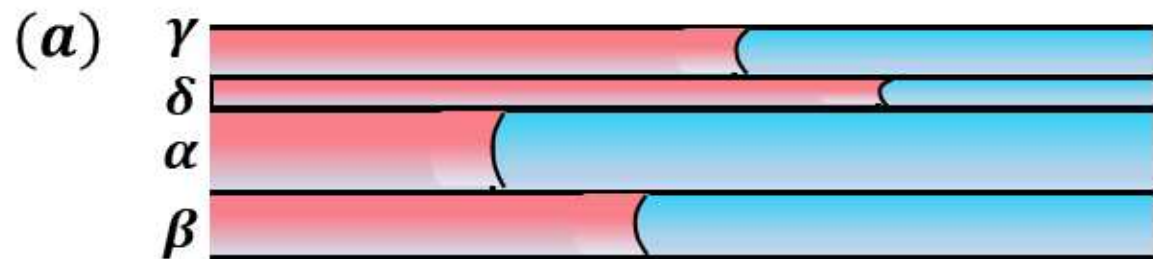
$$z_\gamma > z_\delta > z_\beta > z_\alpha$$



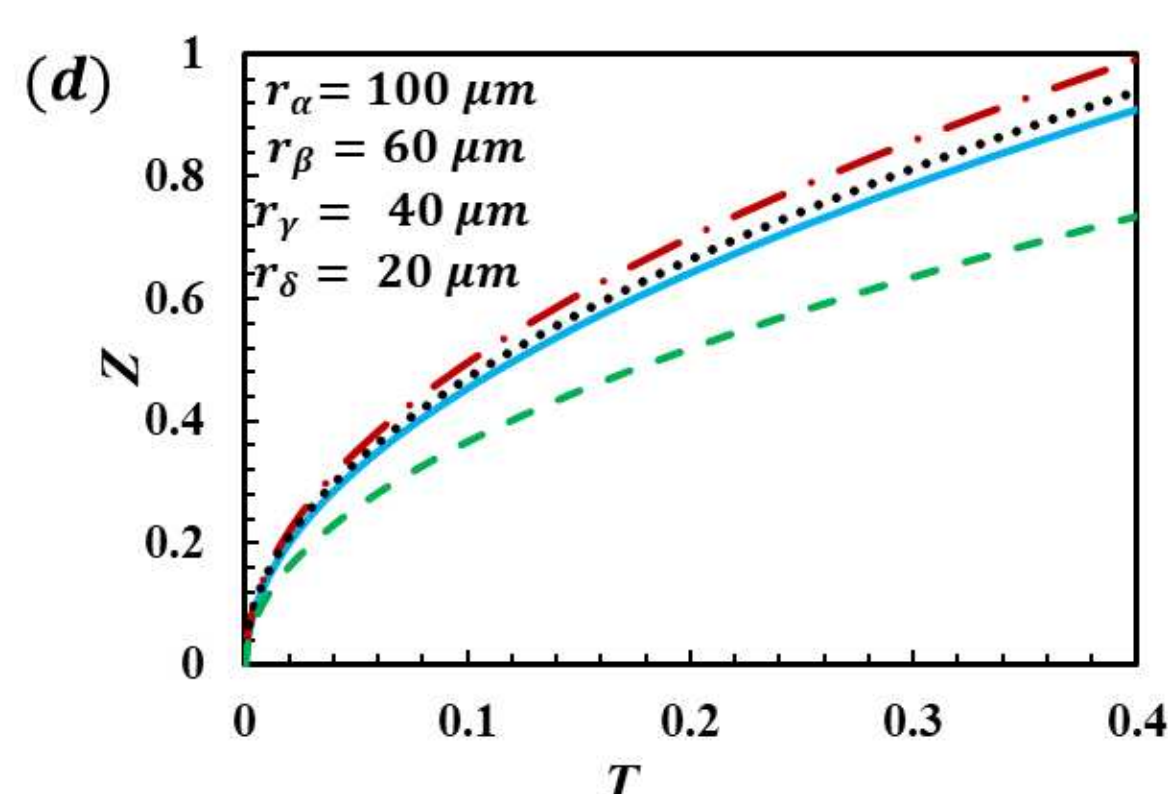
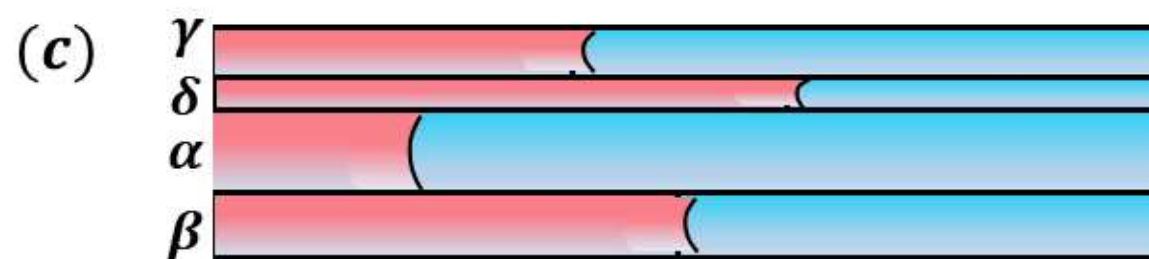
$$z_\gamma > z_\beta > z_\delta > z_\alpha$$



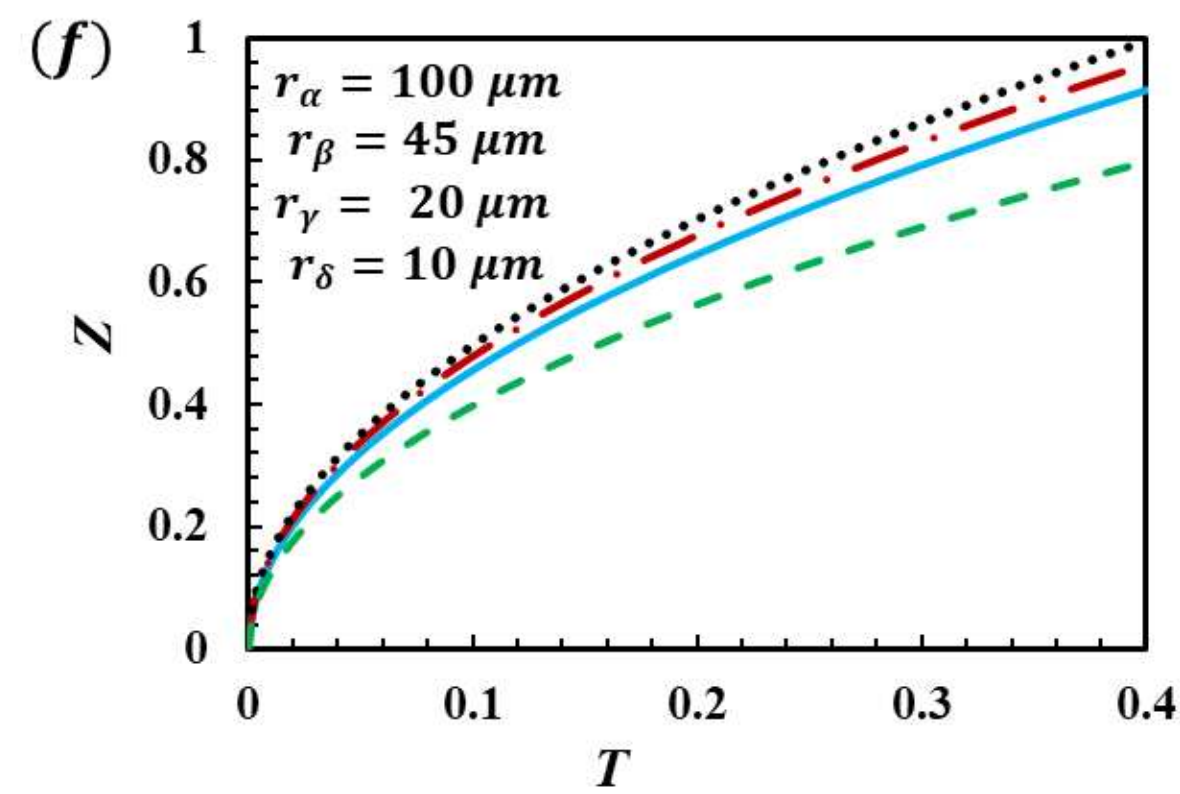
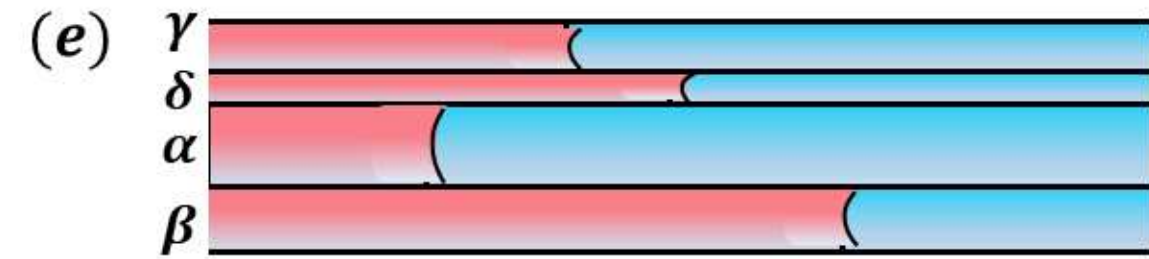
$$z_\delta > z_\gamma > z_\beta > z_\alpha$$



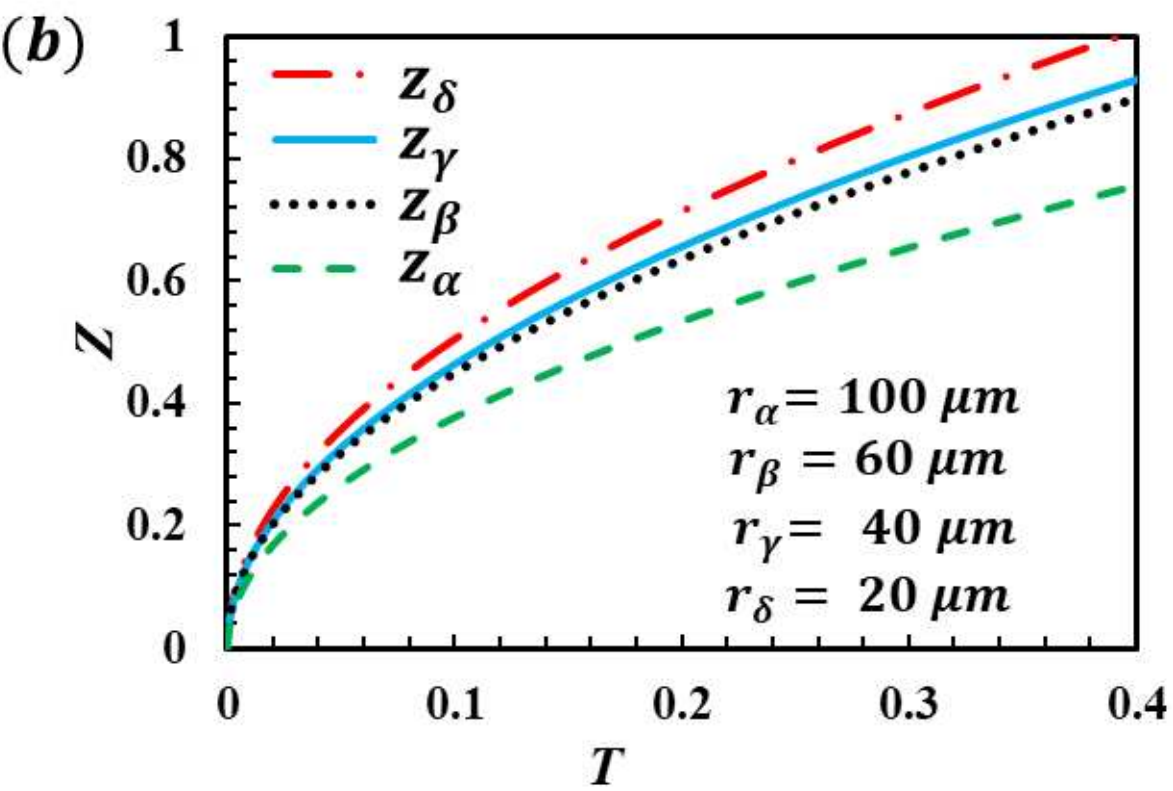
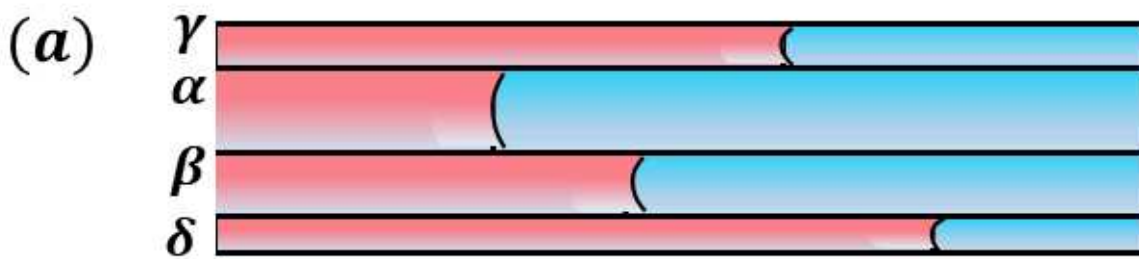
$$z_\delta > z_\beta > z_\gamma > z_\alpha$$



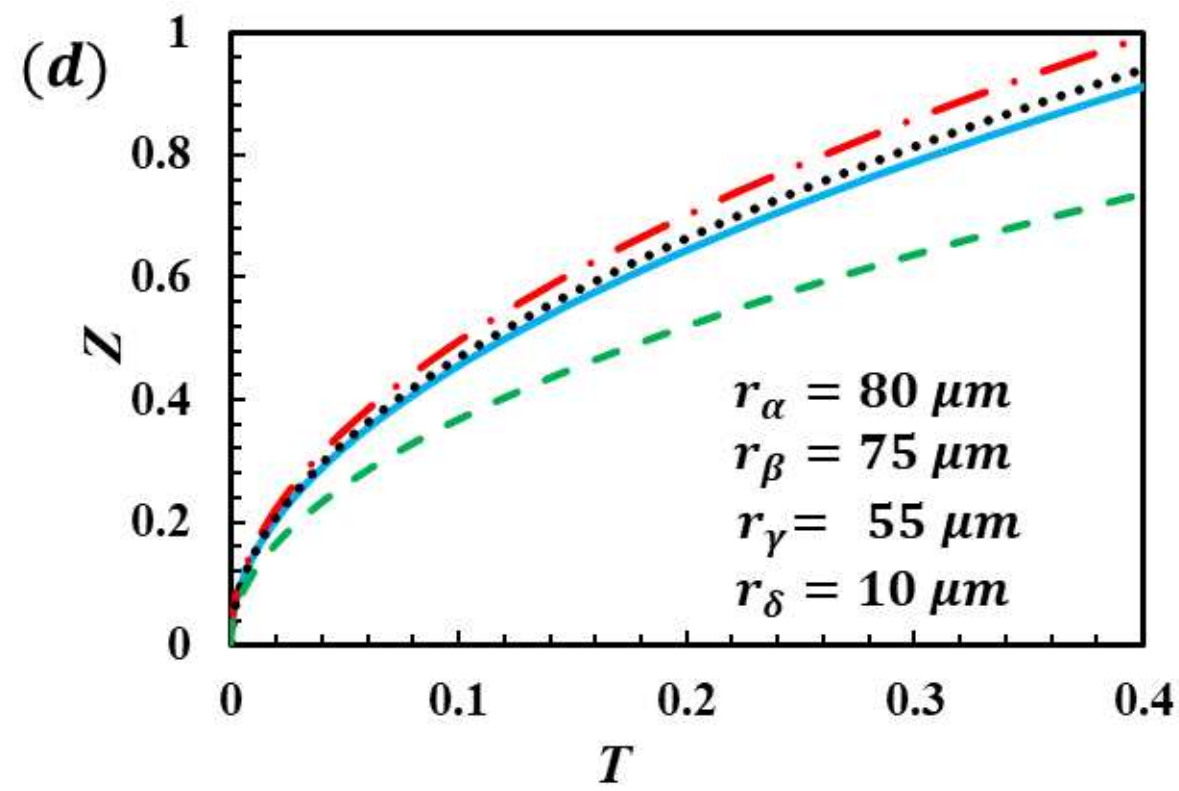
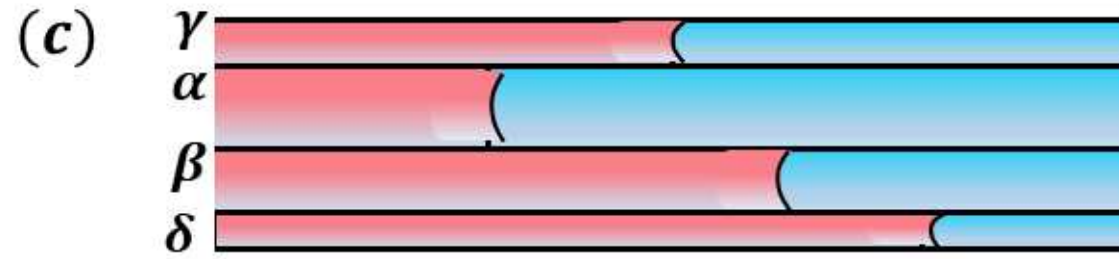
$$z_\beta > z_\delta > z_\gamma > z_\alpha$$



$$z_\delta > z_\gamma > z_\beta > z_\alpha$$



$$z_\delta > z_\beta > z_\gamma > z_\alpha$$



$$z_\gamma > z_\delta > z_\beta > z_\alpha$$

